FACULDADE DE ENGENHARIA DA UNIVERSIDADE DO PORTO

Multimodal Breast Image Registration: Mapping MRI and Surface Data

Pedro Henrique Moreira Queirós Carvalho

U.PORTO

FEUP **FACULDADE DE ENGENHARIA**
UNIVERSIDADE DO PORTO

Integrated Master in Electrical and Computers Engineering

Supervisor: Hélder Filipe Pinto de Oliveira, PhD

Second Supervisor: Sílvia da Conceição Neto Bessa, MSc

July 27, 2018

Resumo

O cancro da mama é um dos mais comuns entre mulheres e cirurgia é quase sempre necessária para o seu tratamento. A mastectomia era a norma, mas hoje em dia outras opções que não removem completamente a mama estão disponíveis, como a Cirurgia Conservadora da Mama. A eliminação de tumores na mama pode ter um impacto na sua estética, mesmo com Cirurgia Conservadora da Mama e, como a mama é importante para imagem corporal e feminidade da mulher, o resultado da cirurgia pode ser devastador para a saúde psicossocial da paciente. Estas repercussões são diminuídas quando a paciente faz parte do processo de decisão do tratamento, o que demonstra a importância de planeamento cirúrgico. Para melhorar a interação entre médicos e pacientes, ferramentas de visualização específicas à paciente ajudariam imenso, ao mostrar previsões de resultados para várias opções de tratamento num modelo 3D ao qual a paciente se consegue identificar. Para este modelo ter a informação interior necessária para o médico analisar o tumor e a informação exterior necessária para a visualização da paciente, registo de imagem multimodal é importante. Ao juntar dados de vários exames, facilita a criação de um modelo 3D completo.

Registo multimodal de imagem da mama é uma tarefa difícil devido às diferentes poses das pacientes quando sujeitas aos exames. O objetivo desta dissertação é combinar a informação de Ressonância Magnética (MRI), adquirida com a paciente deitada virada para baixo, com dados de superfície, adquiridos com a paciente em pé. Os dados de superfície são usados como referência por ter uma forma mais natural e familiar à paciente. Devido à natureza deformável da mama, a forma desta é completamente diferente entre os tipos de dados, significando que rotações e translações não são suficientes para os combinar. Transformações não rígidas, que conseguem alterar a forma dos dados, também são necessárias.

A estratégia de registo seguida é um processo de dois passos. Primeiro, um registo rígido roda, translada e aplica um algoritmo *Iterative Closest Point* para grosseiramente alinhar os dados de MRI com os de superfície. O segundo passo é o registo não rígido, que é feito usando um algoritmo *Free Form Deformation* (FFD) para combinar os dados refinadamente. Em adição à informação original de MRI, a estratégia também é aplicada a simulações bomecânicas da informação de MRI para a posição em pé, que compensa a diferença de pose, tendo uma forma mais parecida à dos dados de superfície. O algoritmo FFD foi testado com grelhas de pontos de controlo 2D e 3D, sendo mais bem sucedido a combinar os dados com as 3D. Os resultados são promissores, com uma distância euclidiana média de 0.83 milímetros quando usadas as simulações biomecânicas e uma grelha de pontos de controlo [8 8 8]. Usar os dados originais de MRI também proporciona bons resultados, mas os melhores são alcançados com as simulações biomecânicas, devido a estas terem uma forma mais aproximada da superfície.

Palavras-Chave: Cancro da Mama; Cirurgia Conservadora da Mama; Resonância Magnética; Dados de Superfície; Registo de Imagem; Registo Multimodal; Iterative Closest Point; Registo Não Rígido; Free Form Deformation.

Abstract

Breast cancer is one of the most common cancers among women and surgery is almost always necessary for its treatment. Mastectomy used to be the standard, but nowadays other options that do not completely remove the breast affected are available, such as Breast Conserving Surgery (BCS). Surgically eliminating tumours in the breast can have an impact on its aesthetics, even with BCS and, because the breast is important for a woman's body image and femininity, the outcome of surgery can be devastating for the psychosocial health of the patient. These repercussions are lessened when the patient is part of the treatment decision process, which demonstrates the importance of surgical planning. To improve the interaction between physicians and patients, patient-specific visualisation tools would help immensely, showcasing the predicted outcomes of various treatment options on a 3D model to which the patient can relate. For this model to have the interior data necessary for the physician to analyse the tumour and the exterior information needed for the visualisation of the patient, multimodal image registration is important. By matching information from different exams it facilitates the creation of a complete 3D model.

Multimodal breast image registration is a difficult task due to the different poses of the patients when undergoing different exams. The goal of this dissertation is to match Magnetic Resonance Imaging (MRI) information, which is acquired with the patient lying face down, and surface data, which is acquired with the patient standing upright. The surface information is used as reference since it has a more natural shape and is more familiar for the patient. Due to the deformable nature of the breast, its shape will be completely different between both types of data, meaning rotations and translations are not enough to match them. Non-rigid transformations, that can alter the shape of the data, are also necessary.

The registration strategy followed is a two step process. First, a rigid registration step rotates, translates and applies an Iterative Closest Point algorithm to roughly align the MRI data to the surface information. The second step is the non-rigid registration, which is done using a Free Form Deformation algorithm (FFD) algorithm to finely match the data. In addition to the original MRI information, the strategy is also applied to biomechanical simulations of the MRI data in the upright position, which compensate for the pose difference, having a more similar shape to the surface data. The FFD algorithm was tested with 2D and 3D control point grids, with the latter being more successful in matching the data. The results are promising, with an average euclidean distance between the matched data of 0.83 millimetres being achieved when using biomechanical simulations and an [8 8 8] control point grid. Using the original MRI data also provides good results but the best were achieved using the biomechanical simulations, due to having a more similar shape to the surface.

Keywords: Breast Cancer; Breast Conserving Surgery; Magnetic Resonance Imaging; Surface Data; Image Registration; Multimodal Registration; Iterative Closest Point; Non-Rigid Registration; Free Form Deformation.

Agradecimentos

Gostava de começar por agradecer aos meus orientadores, Hélder e Sílvia, por me darem esta oportunidade de trabalho num tópico que me interessou muito e me proporcionarem as condições necessárias para o realizar. Um agradecimento especial à Sílvia por sempre se ter mostrado muito disponível para me ajudar no que fosse preciso, o que foi fundamental para conseguir acabar este trabalho.

Obrigado a todos os meus amigos por tornarem estes anos de muito estudo também em anos de muita diversão.

Um grande agradecimento aos meus pais que foram o meu suporte desde sempre, dando-me as possibilidades para poder seguir os meus estudos até esta etapa. Sempre me deram estabilidade, conforto e muita alegria. À minha irmã um obrigado por me conseguir fazer sempre rir. Ao resto da minha família, muito obrigado pelo bom ambiente que sempre me proporcionaram.

O meu maior agradecimento vai para a minha namorada, Rita. Por todo o apoio e palavras de encorajamento que, por vezes, tanto precisei, obrigado. Espero que continues a estar ao meu lado por muitos, muitos anos porque já não sei o que seria a vida sem a tua companhia.

Pedro Henrique Carvalho

"If something is important enough,
even if the odds are against you,
you should still do it."

Elon Musk

Contents

List of Figures

List of Tables

Abbreviations and Symbols

2D   Two Dimensional
3D   Three Dimensional
BCS   Breast Conserving Surgery
FE   Finite Elements
FFD   Free Form Deformation
FLE   Fiducial Localisation Error
ICP   Iterative Closest Point
MG   Mammography
MRI   Magnetic Resonance Imaging
MRIup   Biomechanical Simulation of an MRI to the Upright Position
NURBS   Non Uniform Rational Basis Spline
PCL   Point Cloud
SV   Surface Variance
TRE   Target Registration Error
US   Ultrasound

Chapter 1

Introduction

1.1 Context

Breast cancer has one of the highest incidence rates of female cancer, affecting women worldwide. If it is diagnosed in an early stage, it has a high survival chance, but if found in the later stages the survival rate plummets [8].

The complete removal of the breast, or breasts, affected by the tumour (Mastectomy) used to be prescribed for essentially every case of breast cancer because it is very successful in removing the tumour. Nowadays there are more options, such as breast conserving surgery (BCS) that eliminates only the tumour and a margin of healthy tissue. Although less extreme than mastectomy, BCS can still originate undesired results, leaving the patient with deformities in the breast.

Surgically eliminating tumours in the breast can be very impactful on its aesthetics, which might be devastating for the psychosocial health of women. Loss of self-esteem, sex impairment and dislike towards their own body are some of the consequences women have reported after surgery [1]. Thus, surgical planning for breast cancer surgeries, where the patient and her partner can be part of the decision-making process, is gaining support from physicians. Studies confirm that the mental repercussions arising from the surgery outcome are lessened if the patient is involved in deciding between different treatment options [46]. To facilitate this, breast image registration can be important, since it enables the creation of tools for showing predictions of the outcomes of various treatment options that are unique to each patient, while also presenting interior information important to the physician.

1.2 Motivation

Since so many women are affected by breast cancer [11], it is extremely important to create tools for diagnosis and surgery planning. Patient-specific visualisation tools would be useful and one way to achieve this would be using breast image registration to create 3D models of the breast with interior and exterior information. However, this is a difficult task because images acquired

from different modalities result in different shapes of the same breast. Magnetic Resonance Imaging (MRI) images are acquired with the patient in the prone position (body lying face down) while surface data is obtained with the patient standing upright. By transforming the MRI information using the surface data as a reference, it results in the interior and exterior information of the MRI being in a more natural and relatable shape for the patient, enabling the creation of patient-specific visualisation tools. Despite its importance, few papers have been published on the topic of matching interior radiological images with surface data of the breast.

1.3 Objectives

With the purpose of improving visualisation tools to be patient-specific and complete with interior and exterior information, the main goal of this dissertation is to design an image registration strategy to match MRI and 3D surface data to facilitate the creation of a 3D model of the breast complete with interior and exterior information, different for each patient.

1.4 Contributions

The contributions made by this dissertation are:

- A rigid image registration algorithm to rigidly match MRI and surface information;

- A non-rigid image registration algorithm to finely transform the MRI data with the surface information as reference.

1.5 Structure

This document is split in six chapters, starting with an introductory analysis of the problem.

Chapter 2 is focused on breast cancer, showcasing statistics of the disease, its treatments, repercussions and breast imaging as a way to follow the evolution of the disease. It is also stated how image registration can be an asset in creating tools for breast surgery planning. Chapter 3 is about image registration, giving an overview of how it works in general, followed by a more specific analysis of breast image registration, focusing on radiological surface matching. Methods for validating registration algorithms are also discussed.

In Chapter 4, the main difficulties faced and the approaches used to solve them are examined, while the results are discussed in Chapter 5. In Chapter 6, some conclusions and future work are presented.

Chapter 2

Breast Cancer

Breast cancer happens when cells in the breast begin growing uncontrollably. These cells form a tumour and, if malignant, can spread to other parts of the body (metastasise) or invade surrounding tissue. The grand majority of people affected are women, although a slight percentage are men. Among women, it is the cancer with the highest incidence and one of the highest causes of death from cancer.

The breasts are important not only because of their role in feeding children in their first years, but also because of their role in attracting partners. Patients who survive breast cancer may end up with undesired aesthetic results from surgery, which can be problematic because it affects the mental health of the patient, since the breasts are very important to the self-image, and therefore, self-esteem of women.

In this chapter, general information about breast cancer and its treatments is provided. It is also discussed how the psychological impact in women can be lessened through surgical planning, and how breast imaging can be a tool to facilitate this.

2.1 Cancer Statistics

A study in the United States of America showed that about 1 in every 8 women will be diagnosed with breast cancer in their lifetime. The probability to develop the disease is low in their youth but increases as they get older, as shown in Table 2.1 [8].

Because of this, it is no surprise that breast cancer is, among women, the most common cancer worldwide. In 2012, almost 1.7 million new cases were diagnosed, which accounts for 12% of all cancer cases, and 25% in women.

In Table 2.2, it is shown that, in 2012, there were slightly more breast cancer cases in less developed countries. These countries had 883,000 cases of breast cancer, while, in more developed countries, there were 788,000 cases [11].

Table 2.1: Age-specific probabilities of developing invasive breast cancer for US women (from [8]).

Current Age	10-Year Probability	1 In:
20	0.1%	1,567
30	0.5%	220
40	1.5%	68
50	2.3%	43
60	3.4%	29
70	3.9%	25
Lifetime risk	12.4%	8

Table 2.2: Number of breast cancer cases, deaths and 5-year prevalence worldwide in 2012 (from [11]).

Estimated numbers (thousands)	Cases	Deaths	5-year prev.
World	1671	522	6232
More developed regions	788	198	3201
Less developed regions	883	324	3032
WHO Africa region (AFRO)	100	49	318
WHO Americas region (PAHO)	408	92	1618
WHO East Mediterranean region (EMRO)	99	42	348
WHO Europe region (EURO)	494	143	1936
WHO South-East Asia region (SEARO)	240	110	735
WHO Western Pacific region (WPRO)	330	86	1276
IARC membership (24 countries)	935	257	3591
United States of America	233	44	971
China	187	48	697
India	145	70	397
European Union (EU-28)	362	92	1444

In Figure 2.1, the incidence and mortality rates in 2012 are compared between regions. The highest incidence rates happen in more developed countries, with North America having the highest at 92 per 100,000. In less developed countries the incidence rates are much lower, going as low as 27 per 100,000 in Middle Africa [11].

The mortality rates do not vary as much since the highest incidence regions coincide with the more developed countries, therefore also having higher survival rates. These countries have awareness and screening programmes in place to help detect and diagnose the disease in the early stages, when the survival rates are very high [8].

There are 5 stages of breast cancer, stage 0 being the first and 4 the last. Different breast cancers can be described as: Carcinoma *in Situ* (stage 0), early breast cancer (stage 1 and 2), locally advanced/inflammatory breast cancer (stage 2 or 3) and metastatic/advanced breast cancer (stage 4). The survival rate gets worse as the patients get to later stages [8].

Besides stages, breast cancer can also be classified as non-invasive or invasive. Breast cancer is non-invasive, or Carcinoma *In Situ*, when the cancer is at the point of origin, not invading

surrounding tissue. Invasive cancer grows into and invades healthy neighbouring tissue. Non-invasive breast cancer is at stage 0, having very high survival rates, while invasive encompasses stages 1 through 4 [1].
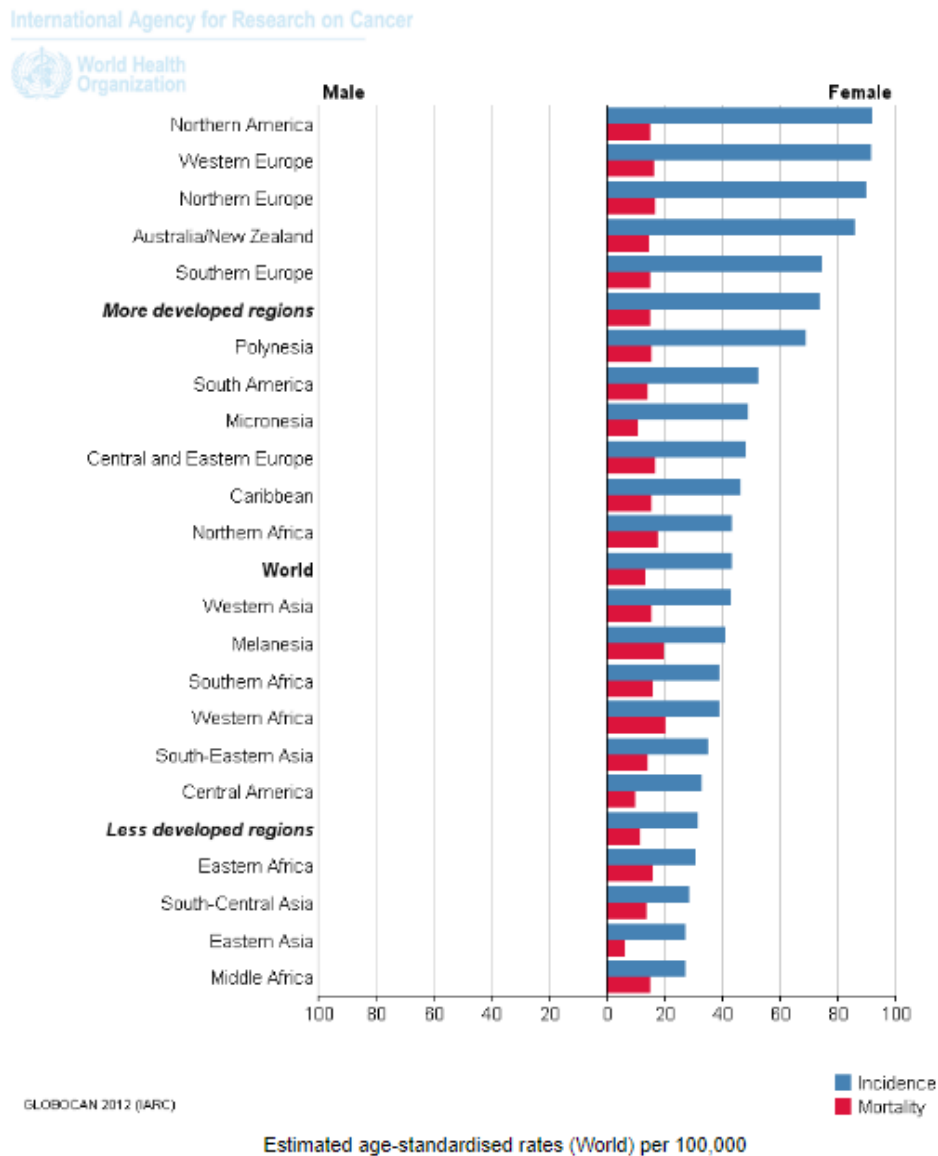
Figure 2.1: Breast Cancer Estimated Incidence and Mortality Worldwide (from [11]).

In Portugal, 6000 new cases of breast cancer are detected yearly and 1500 deaths occur due to the disease[2]. Portugal is one of many countries with a screening programme in place to facilitate the diagnosis of the disease, having done more than 3 million mammographies and forwarded more than 16 thousand women to treatment. Mammography is the gold standard for early detection of the disease [9].

---

[1]http://www.nationalbreastcancer.org/breast-cancer-stages
[2]https://www.ligacontracancro.pt/cancro-da-mama/

2.2   Cancer Treatments

Treatment can be called local if they only affect the tumour area and systemic if the whole body is targeted. The treatment given depends not only on the size and stage of the tumour, but also on the preferences of the patient. Surgery is almost always involved, being either the removal of the breast (mastectomy) or the removal of the tumour and some healthy tissue around it (Breast Conserving Surgery (BCS) also known as lumpectomy) [8].

Before and after surgery, the patient can receive other treatments. These can be chemotherapy, radiation, hormone or targeted therapy, and more than one can be applied. Before surgery, this treatments are called neoadjuvant therapies and their purpose is to shrink the tumour, making the surgery easier and more effective. After surgery, they're called adjuvant therapies and they eliminate cancer cells that might still be in the patients body [25].

2.2.1   Psychosocial Impact of Surgery

Although an extremely important part of breast cancer treatment, surgery often leaves the patient with undesired physical changes. Since the breasts have an important role in sexual attraction and are a symbol of femininity, this changes can be devastating to a woman's psyche and can result in depression, anxiety and a negative impact on sexual health. Studies have shown that women who underwent a mastectomy have more self-image issues than those who had BCS [1]. It has also been shown that women see themselves differently than what outside observers or software measurements might say, so it is important to let the patient be a part of the decision making and surgery planning.

2.3   Breast Imaging

Before, during and after treatments, breast imaging is done to accompany the evolution of the tumour. Different imaging techniques give different and complementary information, therefore, which are used depends on what traits of the breast need to be observed.

There are different categories of imaging techniques, such as radiological, which provide interior information, and 3D surface information, which is exterior. Radiological images are useful for screening and diagnosing breast cancer and for treatment follow-up. 3D surface information is helpful to model the breast and can be used to visualise the appearance of the breast before surgery and predict the aesthetic outcome to help in surgery decision making [27].

2.3.1   Radiological

Radiological exams are important as a non-invasive way of detecting and evaluating breast cancer. Mammography is the gold standard in the screening of the disease. Ultrasounds (US) and Magnetic Resonance Images (MRI) are other common radiological exams used to describe and

classify tumours [2]. They are also important to gather information on the interior of the breast in order to find landmarks to match images of different modalities.

2.3.2 Surface

To assemble surface information, 3D imaging techniques are employed. These can be split in two categories: active and passive. In the former are techniques that project energy on the object and use the reflection to gather the 3D information, while in the latter are techniques that use the energy transmitted from the objects [32]. They can also be classified as direct, when 3D coordinates are immediately provided, or indirect, when processing is needed to get the coordinates. Techniques can be further categorised as either optical or non-optical. In optical techniques the information is carried by light while non-optical measure the time a wave takes to reflect from the object [39].

Common 3D imaging techniques are stereo vision, time of flight sensors, structured light depth sensors and laser triangulators [26]. Breast surface imaging has largely used 3D laser scanning using triangulation or photographs in conjunction with stereo vision. In recent times, RGB-D sensors like the Microsoft Kinect, which is a structured light depth sensor, showed potential in clinical practice [27].

2.4 Surgery Planning

Throughout the years, survival rates for breast cancer became better and better due to screening programmes and advancements in therapies and the result is that most women with the disease will survive. This means that many women will have to live with the repercussions of the treatment. However, studies show that these consequences can be less impactful if the patient is part of the treatment decision process [46]. Therefore it is important to create or improve tools for surgery planning that help communication between doctors and patients. The visualisation of various surgery outcomes is one of these tools, but currently, it is done with images of other patients or using generic 3D models and 2D drawings of women torsos, without personalisation, which makes it difficult for the patient to project herself onto the drawings and leads to wrong expectations. A simulator that is patient specific would be a big upgrade for surgery planning and communication between patient and doctor, resulting in better educated patients and surgical procedures that take into account the patient's wishes as well as clinical limitations [5].

2.5 Summary

Breast cancer is a common disease worldwide and many women will have to live with the physical repercussions of surgery, which is usually part of the treatment. Even with BCS, the breast suffers deformation, which may have a negative psychological impact on the patient. Studies show that women are likelier to accept the results of surgery if they are included in the decision process.

This is why it is important to create tools to help surgeons show the patient what the surgery outcomes will be, depending on different treatment choices. In order to conceive a patient specific software to visualise surgery outcomes, image registration is crucial. It can be used to merge radiological images and 3D surface information, so that both exterior and interior information are available in the same place. In the next chapter, image registration is discussed.

Chapter 3

Image Registration

Image registration is necessary when there is a need to merge the information of two or more images. In the context of breast cancer, image registration can be used to fuse images obtained from different imaging techniques. It is a subject highly discussed in the field of medical image analysis because of its difficulties in matching images of dynamic objects, which is the case for the human body [28]. The objective of image registration algorithms is to align images in the same coordinate system. To achieve this it is necessary to choose a geometric transformation based on the type of information. Most medical image registration algorithms are non-rigid due to the deformability of the human body, but they can also be rigid [34]. Breast image registration is an especially difficult task because breasts are highly deformable, inhomogeneous and anisotropic [13]. Nevertheless, different modalities of images need to be combined to create a complete 3D model of the breast, particularly interior and exterior information.

In this chapter, image registration will be discussed, starting with an overview of registration strategies and then focusing on radiological surface matching in the context of breast cancer.

3.1 Overview

In order to visualise and analyse information from various images of the same object, from different times, angles or acquisitions, image registration is needed [13]. For two images, A being the fixed image and B the moving image, image registration works by using a spatial transformation, τ, that is applied to the moving image B to align its points with the corresponding ones in the fixed image A. A similarity measure S is used to compare both images [44]. Mathematically, the registration of two images can be described as:

$$\hat{T} = \arg\min_{\tau} S(A, \tau(B)) \tag{3.1}$$

Registration of more than two images works the same way, with one being the fixed image for reference and the others the moving images. To evaluate the transformation, two measures are analysed: regularisation (or internal forces), which measures the regularity of the transformation, and data dissimilarity (or external forces), which measures how well τ combines the images [44].

A similarity measure S, feature space, transformation type and search strategy (optimisation) are necessary for image registration and many methodologies have been proposed. These can be classified using nine major criteria: dimensionality, nature of the registration basis, nature of transformation, domain of transformation, interaction, optimisation procedure, modalities involved, subject and object, each with their own sub-criteria. Dimensionality is categorised according to the dimensions of the images, nature of the registration basis depends on the content of the images used for matching while the nature of the transformation classifies the algorithm depending on the type of transformation. The domain of the transformation can be global, if the complete image has one transformation, and local, if parts of the image have different transformations. Interaction represents how much the user can influence the registration algorithm. Regarding the optimisation procedure, the algorithm is classified on how the parameters are found. Modalities involved categorises the number and type of imaging modalities used for the registration, subject dictates if the images are from the same or different subjects and the object is the content of the images [28].

The transformation nature chosen dictates the parameters of τ and classifies image registration algorithms as rigid or non-rigid. The former includes rotation and translation, having six degrees of freedom in a 3D space, while the latter accounts for the similarity (translation, rotation and uniform scaling), affine(translation, rotation, scaling and shear), projective (any deformation as long as lines continue straight) and curved (or deformable) transformations. In medical image registration, rigid transformations are mainly used for rigid structures (such as bones) or for pre-registration to be followed by a non-rigid transformation, which are more common in this field due to the deformable nature of most of the human body. [28].

Regarding the feature space, registration methodologies are differentiated regarding the image information used, which can be raw voxel intensity, statistical information of the voxels, intensity gradient or features of the image, such as surfaces, points, edges and volumes [28]. The similarity function uses this information to match the images and algorithms are commonly divided in intensity-based, if they depend on voxel intensity, or feature-based, if they use extracted geometrical structures from the images [44].

In Figure 3.1 a general framework of image registration is shown. The fixed image A is compared to the moving image B, that underwent a transformation, using a similarity function. The algorithm then checks if the similarity measure coincides with the stop condition. If it does not, a search strategy calculates new parameters for the transformation and B undergoes another one. This cycle continues until the stop conditions are met and the registration information is outputted for validation [28].

Image registration problems can have different solutions depending on the selection of moving and fixed images, due to local optimums of the chosen similarity measure [28]. The optimisation algorithm has the objective of minimising or maximising this measure, until it meets the requirements needed. Common strategies are exhaustive search, simple gradient descent, simulated annealing, conjugate gradient descent and Newton-Raphson [41]. A regularisation model R can be used to restrict what the result can be and filter out unwanted solutions [42]. The registration
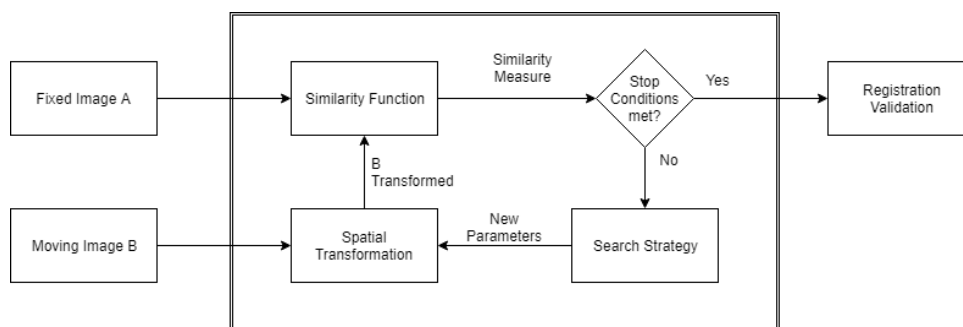
Figure 3.1: Typical algorithm for image registration (adapted from [28, 45]).

problem can be altered to accommodate this:

$$\hat{T} = arg\min_{\tau}(S(A, \tau(B)) + R(\tau)) \tag{3.2}$$

This way there are fewer possible transformations that are more in line with the desired outcome. Properties that affect the type of transformation are: smoothness, bijectivity, invertibility or diffeomorphism. A transformation is smooth when its partial derivatives, until a certain order, exist and are continuous. It is bijective when points are mapped one to one. When a transformation is bijective and continuous, while having a continuous inverse, it is invertible. An invertible and smooth transform is called diffeomorphic. While smoothness is required to keep the morphology of the images, the other properties are conditional. Bijectivity prevents folding of the images, invertibility is needed to map images from a set to the same space and diffeomorphism maintains the topology of the images. Depending on the images to be registered, the transformation can have these properties or not [44].

3.2   Radiological Surface Registration

Radiological imaging of the breast is extremely important to follow the evolution of breast cancer in a patient, since the detection until after the treatments. To complement the information of the mammography acquired during the screening of the disease, ultrasound and MRI are obtained to accurately characterise the tumour. Registration of these exams facilitates their interpretation by combining all the data in a single referential. It is also important to align different views of the same modality.

Surface reconstruction is needed to obtain an authentic 3D model of the breast. Registration is used to combine point clouds (PCLs), which is a common output of surface imaging sensors, of multiple views to reduce noise and result in a more complete 3D representation.

With image registration it is possible to merge radiological and surface information to create a model with complete interior and exterior data.

3.2.1   Radiological Registration

Breast radiological imaging is always present throughout the treatment of breast cancer. Mammographies are done for the screening of the disease and, if a tumour is found, ultrasounds and MRIs are obtained to better identify its stage, position and size. Inter-modal (or multimodal) registration can be applied to merge all the complementary information of these different exams, resulting in an image with all the important information.

Intra-modal registration is mostly used to align images from exams done at different times. This is a very difficult task since the position of the patient is different every session and she might have experienced physical changes. This problem is shared by intra and inter-modal registration. There is also work done with intra-modal registration of images from the same time but taken from varying angles [18, 19]. Methods for intra-modal mammography registration have been proposed but the results have not been very accurate due to the compression of the breast in the exams [15]. Because of this, the 3D shape of the breast is given by the MRI, which has less compression. Studies on intra-modal MRI registration have shown that non-rigid or hybrid methods are more accurate than rigid or affine [33, 35, 40]. Although there is some work done on ultrasound registration, it is not a popular research topic, being more complex than for other imaging techniques.

Inter-modal registration has been primarily applied between mammographies and MRIs. This is useful to repair the deformation applied to the breast during the mammography by merging with MRI information, which is closer to the 3D shape of the breast. Mammography is usually used instead of other imaging techniques because it is easier to process its information. Several papers have been published on the topic of MRI and mammography registration, proposing a variety of solutions to the problem with good results [20, 23, 24, 36]. However, there is still room for improvement because of the difficulty in achieving an optimum solution.

3.2.2   Surface Reconstruction

Surface 3D information is usually obtained as PCLs from an imaging sensor. The choice of sensor used can influence the difficulty of the surface reconstruction. The requirements of the results are dictated by the target application, also influencing the difficulty of the operation. The PCLs resulting from the sensors are already a 3D surface representation, being a set of 3D points. However, to create a less noisy and more complete 3D representation, registration of multiple PCLs of the object, from different angles, is done [43]. To conclude the surface reconstruction, the final PCL is converted to a 3D surface.

On the topic of breast surface reconstruction, Costa et al. [6, 7] has proposed a coarse registration method based on tesselation, using the Delaunay Triangulation principle to extract robust keypoints from the RGB-D sensor information. After these points are selected, a version of ICP (iterative closest points) algorithm is used to align the different views. The results are promising, needing only three views and reconstructing the torso in practicable time.

3.2.3   Radiological Surface Matching

Most breast image registration work has been done with intra and inter-modal radiological images to characterise the interior of the breast. Surface reconstruction of the breast has also been reasonably researched. However, there is very little exploration of interior and exterior information matching, in order to create a complete model of the breast. Regarding interior registration, MRI is usually the reference other radiological images are transformed to, since it has the least deformation and originates a good 3D representation of the interior of the breast. The exterior information is reconstructed from a 3D PCL to achieve malleable surfaces. Thus, image registration between interior (radiological imaging mapped to a MRI reference) and exterior (surface reconstructed from a PCL created by a sensor) information results in a complete 3D model of the breast.

The important task of interior and exterior matching is very difficult due to the highly deformable nature of the breast. The differences in pose between interior and exterior acquisitions are a major challenge. Since surface information is obtained with the patient in the upright position while for MRI the patient is in the prone position (lying horizontally face down), the breasts present different shapes. Therefore, a pose transformation is needed in order to complete the registration. Biomechanical models are physical models that have been studied to characterise the breast shape changes when in different positions [21, 30, 31]. Figure 3.2 illustrates how the breast changes shape depending on the pose of the patient.

Figure 3.2: View of patients breasts in different poses. Left image obtained in the upright position, middle one at 45 degrees and the last one in the supine position (from [31]).

Other factors influence the shape of the breast, such as the position of the arms, which are upward during MRI and at the side of body or on the waist when acquiring surface information.

The topic of pose transformation has been researched, in particular, prone to supine (lying horizontally face up) registration with the objective of using MRI images to aid in breast surgeries, since they are done with the patient in the supine position [14, 4]. Solutions for this problem have been suggested, using physical or non-physical models.

Breast image registration using physical models based on finite element (FE) methods are common, usually for radiological registration [16]. Yet, physical models have drawbacks, such as a high computational cost and difficulty to define some parameters, which can be unknown. These has lead to researchers studying physical models in combination with other methods of registration. An example is the work of Eiben et al. [10], which uses FEs based biomechanical models in conjunction with a surface registration algorithm to match prone and supine MRI images as well as MRI and surface images acquired with the patient upright. From a prone position MRI, a biomechanical model is applied, followed by an update of the unknown parameters of the model using the supine or upright surface images. Then an ICP algorithm is used to match the skin from the biomechanical model with the surface images. Salmon et al. [38] also resorted to biomechanical models for pose transformation, in order to combine MRI and surface imaging information. This research accomplished the objective of retrieving a reference state of the breast by applying FEs biomechanical models to interior and exterior data and then aligning both by adjusting parameters.

Regarding non-physical models, many parametric models have been researched. The use of Non Uniform Rational Basis Splines (NURBS), deformable models obtained from combinations with free form deformation (FFD) or registration based on ICP and reference points are examples of non-physical strategies [35, 29, 17]. Nonetheless, these are less accurate than physical models for registration of images from different views, but they can be used together to obtain better results than each one individually [22]. NURBS, B-splines and Bézier curves are methods that uses splines to represent objects and adjust them with a set of control points. FFD also uses points to control object representation but deforms the object indirectly by modifying the space it is in. The object is enclosed in a parallelepipedic grid, with each vertice being a control point that will modify the object when adjusted. ICP is an algorithm that iteratively matches the closest points between to PCLs and transforms the moving image to minimise the distance between them. The original ICP only applied rigid transformations but there have been many variants of the algorithm proposed.

3.3   Validation Methods

In order to be accepted, a new strategy needs to be validated, especially when its application might be clinical, but it is difficult to evaluate a registration accuracy when the ground truth is usually unavailable [13]. The similarity measure could be a rough approximation of accuracy, since a registration problem can be defined as an optimisation problem [28], but the possible lack of geometric significance of the similarity measure requires better evaluation. Visual inspection is

usually a qualitative measure of registration results, however its subjectivity is a drawback. Thus, there is still a search for better accuracy measurements [40].

Image registration quantitative evaluation can fall on two classes: synthetic or real. The former uses simulated ground truths, while the latter uses fiducial points or extrinsic markers on real data.

Synthetic validation can be done by starting with two identical images and applying a known transformation to one. Then the registration algorithm is applied to the other image and the results compared, being the first deformed image treated as ground truth [28, 44]. Metrics used to compare images are image subtraction, dice similarity coefficient and distance computations for intra-modality registration. In inter-modality statistical metrics have to be used, for example, mutual information. Another synthetic approach is to simulate the acquisition conditions of the images and test the registration strategy on these synthetically created images [40].

Evaluation using real data works by marking points in the input images, using fiducial markers for example, applying the image registration and comparing the points marked in the outcome [44]. Target registration error (TRE) evaluates the accuracy of the registration using the Euclidean distance between the highlighted points. To evaluate if the markers are well positioned, the fiducial localisation error (FLE) is used.

3.4 Summary

Image registration is a process that merges and aligns two or more images to the same coordinate system. It is an optimisation problem with the objective of minimising a cost function, dictated by the similarity measure, and finding the ideal transformation. Registration algorithms can be divided in rigid and non-rigid. For medical image registration, non-rigid registration is almost always needed due to the deformable nature of most of the human body, although rigid transformations can be used as pre-registration to initially approximate the input images.

Inter-modal radiological registration is a popular research topic, but little has been done in matching interior radiological information with 3D surface data. FE deformable methods have been proposed as physical models for image registration, but they have high computational complexity. Parametric models can be an alternative, having lower complexity but still being able to align images. While breast surface reconstruction solutions are available, the same cannot be said for the problem of 3D surface and radiological registration. This is a difficult task due to the different positions of the patient when the information is acquired, during radiological exams and surface data acquisition, which lead to varying breast shapes. The absence of clear landmarks between surface and interior data and of an optimum validation strategy also help to make this registration problem a difficult one.

Chapter 4

Methodology

The objective of this dissertation is to match breast MRI and surface information, which facilitates the creation of a 3D model complete with interior and exterior data. The main difficulty comes from the difference in poses when acquiring the data (prone for the MRI and upright for the surface). The lack of rigid structures in the breast results in different poses leading to different shapes of the breast. The equipment of the MRI also slightly compresses the breast, applying further deformation. Another difficulty is the lack of points of reference besides the nipple, which, in a post surgery situation, might not be present.

In order to solve this problem, a rigid registration is necessary, followed by a fine non-rigid registration, since rigid transformations alone are not capable of compensating for the pose difference. A good rigid registration helps to ensure that the fine registration will produce good results. Throughout this chapter,the methods used are explained and discussed. The next section describes the data set.

4.1 Data

The inputs for this methodology are the MRI and surface data. MRI results in sets of images, where each is a slice of the patient's torso. MRI images are then segmented to generate a PCL of the breast contour, as shown in Figure 4.1. The surface data derives from the work of Costa et al. [6], which reconstructs 3D surface information acquired using the Microsoft Kinect. Surface information is represented by PCLs. Figure 4.2 shows an example of the data in its initial state. It also exposes how the data is oriented. Regarding the surface data, the Z-axis is positive in the anterior $\rightarrow$ posterior direction, which means the front of the body is in the direction of -Z, the Y-axis is positive in the inferior $\rightarrow$ superior direction, meaning the head is in the direction of +Y, and the X-axis is the laterality, being positive from left to right. As for the MRI data, the Z-axis is positive in the inferior $\rightarrow$ superior direction, the Y-axis is positive in the anterior $\rightarrow$ posterior direction and the X-axis is positive from right to left.

Since each MRI image is a slice of the torso, the resulting points are unevenly distributed, appearing in layers, so, in order to have a more even distribution, the MRI PCLs are downsampled.
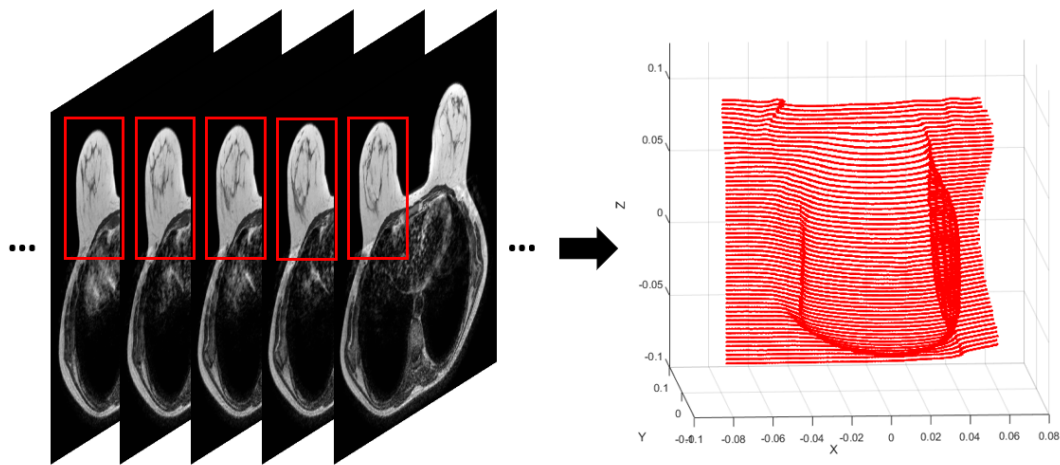
Figure 4.1: Initial MRI images and the resulting PCL.

Originating from the work of Zolfagharnasab et al. [47], biomechanical simulations of the MRI in the upright position are also used. Based on work done on the topic of aligning breast images acquired in different poses [14, 38], there is reason to believe using biomechanical models will provide good results. From this point on, these simulations will be referred to as MRIup. The downsampled MRI/MRIup PCLs used come from the dataset of [47], which is composed of twelve breasts from seven patients (two of which only have data of one breast). Figure 4.3 exposes an initial MRI PCL, a downsampled MRI PCL and its respective MRIup and surface PCLs. It can be observed that the biomechanical model is closer in shape to the surface, but still in the same referential.
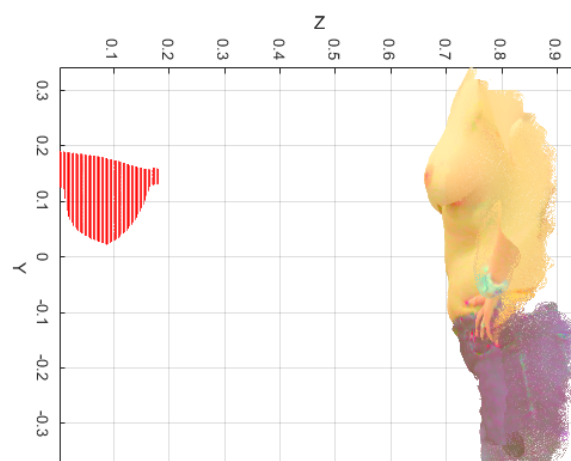
Figure 4.2: PCL generated from segmentation of MRI images (on the left) and Surface PCL (on the right).

(a) Segmented MRI.

(b) Downsampled MRI.
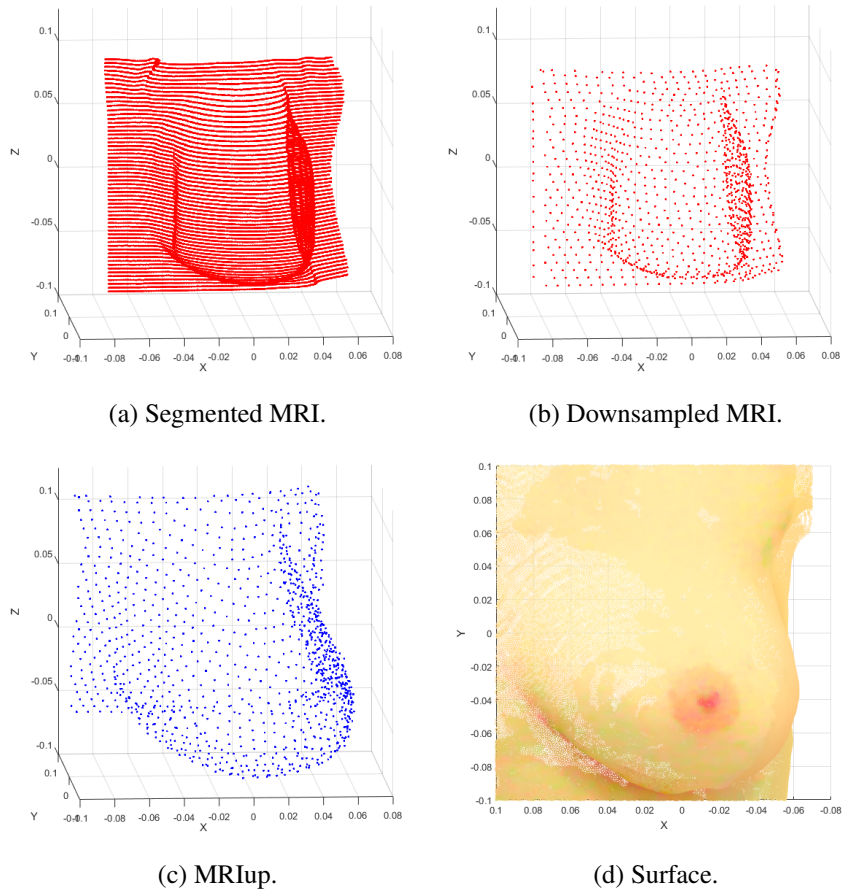
(c) MRIup.

(d) Surface.

Figure 4.3: Comparison between segmented MRI data, downsampled MRI data, MRI data after biomechanical simulation and surface data.

The transformations that are involved in this methodology are applied to both MRI/MRIup using the surface as the reference. The goal is to compare the registration using both MRI/MRIup PCLs, since there is work done on the topic [14] showing that biomechanical modelling before the registration algorithm leads to better results.

4.2 Rigid Registration

The rigid registration comprises a rotation, translation and an ICP algorithm to approximately align both MRI/MRIup with the surface data, as shown in Figure 4.4.

4.2.1 Rotation

First, the MRI/MRIup data is rotated to ensure the same orientation as the surface. This is done assuming the input data always comes in the same orientation, which can be expected since the MRI images are almost always acquired the same way. Therefore, the rotation is as simple as

Figure 4.4: Flowchart of the rigid registration step.

rotating the MRI PCL -90° along the X-axis and 180° along the Z-axis. The MRI metadata can also be examined to extract the orientation of the patient during the exam.

4.2.2 Translation

The translation is done by detecting the nipple on the MRI/MRIup and surface data and translating the MRI/MRIup PCL to match the points found. The nipple has high curvature so, to detect it, the surface variance (SV), which is an approximation of curvature, is used [37].
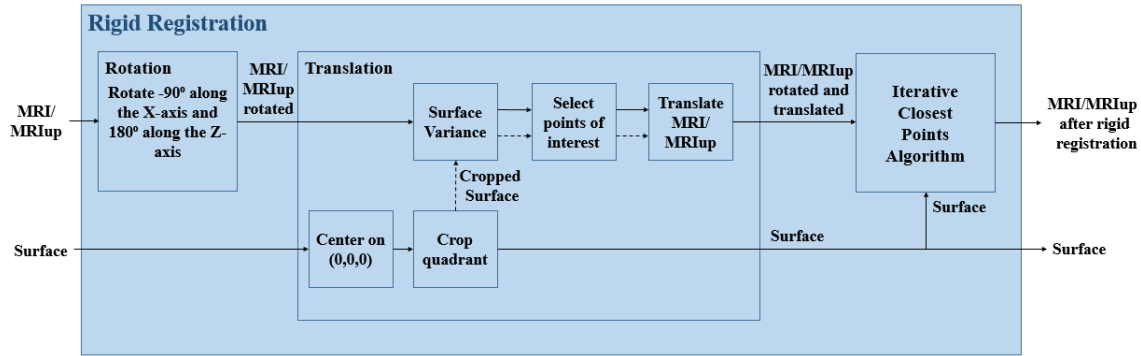
The SV is calculated at each point on both MRI/MRIup and surface PCLs, and the points below a certain threshold are discarded, since a small value of SV indicates a point is on the same plane as its nearest neighbours. Equations 4.1 and 4.2 show how the SV σ_p of a point p is derived from the eigen values λ_n of the covariance matrix C, where k is the number of neighbours and $\lambda_0 = \min \lambda_n$ [37].

$$C = \frac{1}{k} \sum_{i=1}^{k} (p_i - \bar{p})(p_i - \bar{p})^T \tag{4.1}$$

$$\sigma_p = \frac{\lambda_0}{\lambda_0 + \lambda_1 + \lambda_2} \tag{4.2}$$

Finally, the minimum along the Z axis (anterior $\rightarrow$ posterior axis) is found among the selected points in both PCLs and the MRI is translated to match the points detected. This way, the selection is only between points with significant SV and the minimum along the Z axis will be the nipple or in the area close to it.

In some cases, points on the abdomen were being detected so, to minimise the probability of detecting the wrong area, the surface PCL centroid is translated to the coordinate system's origin $(X, Y, Z) = (0, 0, 0)$ and only the points on the quadrant containing the breast are selected at the start of the detection algorithm.

4.2.3 Rigid Iterative Closest Point

For better approximation between both PCLs a rigid ICP algorithm is applied. The ICP function *pcregrigid* from Mathworks Matlab R2016a Computer Vision System Toolbox version 7.1 is used, which iteratively determines a translation and rotation to minimise the distance between the PCLs, calculated between each MRI/MRIup point and its closest point in the surface plane, which is computed using the normal vectors of each point. The algorithm computes the average difference between the transformations of the previous three iterations and stops when it is below the tolerance values for the translation and rotation differences, the former being the euclidean distance between translation vectors and the latter the angular difference in radians. It can also stop if it reaches the maximum number of iterations.

4.3 Non-Rigid Registration

Due to the deformable nature of the breast, rigid transformations are not enough to compensate for the differences in shape between the MRI and Surface data. For this reason, non-rigid registration is necessary. A Free Form Deformation algorithm was chosen to finely match the rigidly transformed MRI/MRIup data to the surface, because there is work done in matching data with FFD showing promising results [48, 14].

4.3.1 Free Form Deformation

The flowchart of the FFD algorithm is represented in Figure 4.5 and it is based on the work of Zolfagharnasab et al. [48] and Bardinet et al. [3]. It is an iterative process that gradually deforms the MRI PCL to match the surface.
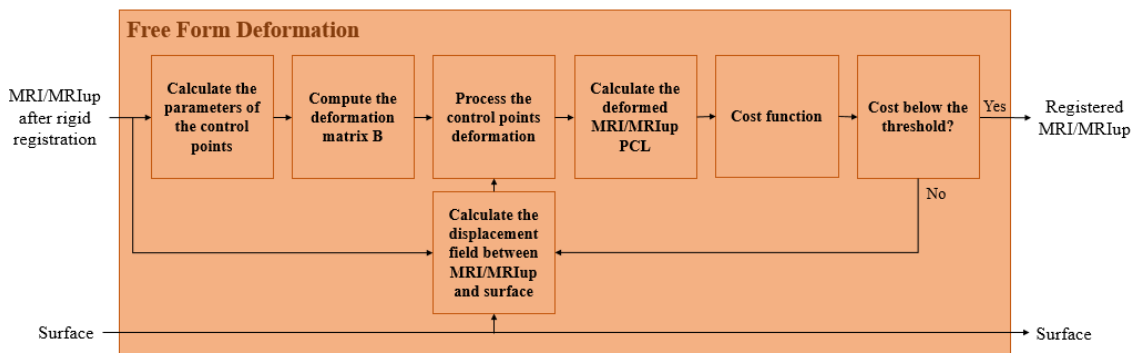
Figure 4.5: Flowchart of the Free Form Deformation algorithm.

The algorithm starts by determining the parameters of the initial grid of control points P with $l \times m \times n$ points around the MRI/MRIup PCL. The eigenvalues and eigenvectors of the MRI/MRIup data are calculated, the dimensions of the grid are computed using the eigenvalues and the orientation of the grid is determined using the eigenvectors to find the Euler angles of

the data. The local coordinates of the MRI points in reference to the grid of control points (s, t and u) are computed using these parameters. The MRI/MRIup points are linked to the control points using a deformation matrix B, which is a product of trivariate Bernstein polynomials. Equation 4.3 shows how the deformation matrix is calculated.

$$B = \sum_{i=0}^{l} \sum_{j=0}^{m} \sum_{k=0}^{n} C_l^i C_m^j C_n^k (1-s)^{l-i} s^i (1-t)^{m-j} t^j (1-u)^{n-k} u^k \tag{4.3}$$

In order to deform the control points grid, a displacement field δX between the MRI/MRIup and surface data is calculated. A $X_z^a = X_z + \delta X$ is computed, with X_z being he MRI/MRIup data on iteration z, and the new control points are determined by a minimisation problem:

$$P_{z+1} = \min_{P} \|BP - X_z^a\|^2 \tag{4.4}$$

This way the control points can move freely and irregularly, so a regularisation term based on [12] is added to preserve the relative position of the points. The minimisation problem, with D_μ being a matrix representing the discretised derivative of the control points position, becomes:

$$P_{z+1} = \min_{P} \{\|BP - X_z^a\|^2 + \|D_\mu P\|^2\} \tag{4.5}$$

The deformed MRI is then:

$$X_{z+1} = BP_{z+1}; \tag{4.6}$$

The FFD algorithm stops when the mean euclidean distance between the MRI of the current and the previous iteration falls below a chosen threshold. The algorithm can also stop if a maximum number of iterations is reached.

4.4 Evaluation Metrics

To evaluate the accuracy of the results, two metrics are calculated between the MRI/MRIup and surface PCLs: the mean euclidean distance and the Hausdorff distance. The mean euclidean distance is the average distance between each point in a PCL and its closest point on the other, while the Hausdorff distance is the maximum among this distances. Equation 4.7 shows how the Hausdorff distance is calculated, with M and S being two PCLs and $\|.\|$ being the euclidean distance.

$$H(M,S) = \max_{m \in M} \min_{s \in S} \|m - s\| \tag{4.7}$$

These distances can be measured in two directions: MRI $\to$ Surface and Surface $\to$ MRI. Due to the surface PCL having a bigger area, calculating in the direction Surface $\to$ MRI results in disproportionate errors, as illustrated by Figure 4.6, using the Hausdorff distance as an example. Therefore, only the distances in the direction MRI $\to$ Surface will be considered.
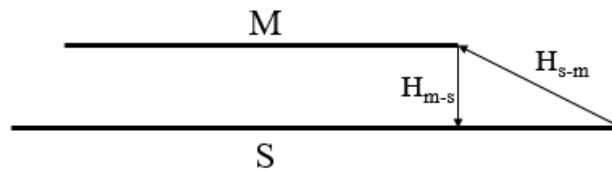
Figure 4.6: Hausdorff distance between two sets of data, M and S, in both directions.

The mean euclidean distance is important to determine how close the two PCLs are overall, while the Hausdorff distance exposes the worst case.

4.5 Summary

To compensate for the different shape of the breast between MRI and surface data inherent to the pose of the patient when acquiring the input data, a rigid registration step is needed, followed by a non-rigid one.

The rigid registration phase comprises of a rotation, a translation and a rigid ICP algorithm. The rotation assures the same orientation of the MRI/MRIup and surface data. The translation of the MRI/MRIup to the surface data is done using an automatic detection of the nipple. The ICP algorithm iteratively translates and rotates the MRI/MRIup data to rigidly align it with the surface data.

The non-rigid registration step is a FFD algorithm that utilises control points around the MRI/MRIup data to deform and finely it match the surface PCL.

In the following chapter the results of this methodology are exposed and discussed.

Chapter 5

Results and Discussion

The methodology explained in the previous chapter is a two step process. The first step is a rigid registration comprised of a rotation, translation and an ICP algorithm. It is done with the intention of rigidly approximating the MRI/MRIup information with the surface data. The second step is the non-rigid registration, which finely matches the data using a FFD algorithm.

The method was tested on a sample of twelve breasts from seven patients. The seven surface PCLs and twelve MRI/MRIup PCLs originate from [47]. To implement the methodology, Mathworks Matlab R2016a and it is run on a computer with a 2.40 GHz processor and 6 GB of RAM. The results of each step are exposed throughout this chapter. The images shown use the left breast of patient 1 as an example, unless specifically stated that it is of another patient. The distance values are shown in millimetres and computation times in seconds.

5.1 Rigid Registration

The initial position of the data is shown in Figure 5.1. It is noticeable that the MRI/MRIup PCLs are not aligned with the surface, needing rotation and translation.

The surface data has the anterior to posterior direction being in the Z-axis, while for the MRI/MRIup data the Z-axis is positive in the inferior to superior direction. The Y-axis is positive in the inferior to superior direction for the surface information, while for the MRI/MRIup data it is in the anterior to posterior direction. The X-axis is the laterality for both, being positive in the left to right direction regarding the surface, and right to left for the MRI/MRIup.

5.1.1 Rotation

Applying a rotation of -90° along the X-axis and 180° along the Z-axis so that the PCLs have the same orientation results in Figure 5.2.
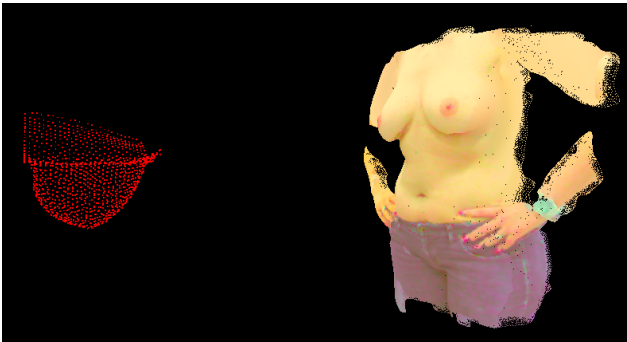
(a)
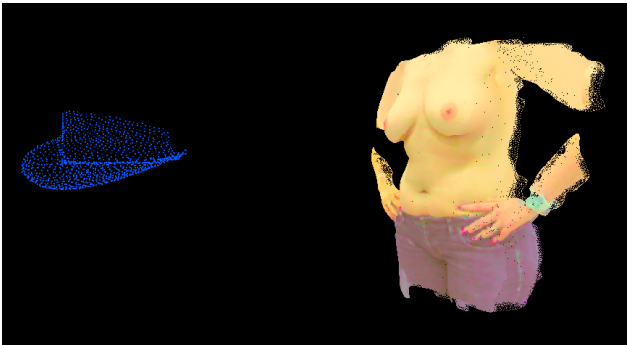
(b)

Figure 5.1: Surface (natural colour) and MRI/MRIup (red/blue respectively) initial data.

(a)

(b)

Figure 5.2: Surface (natural colour) and MRI/MRIup (red/blue respectively) data after rotation.

5.1.2 Translation

The translation described in the previous chapter, using an automatic detection of the nipple, was compared with a translation using manual annotations of the nipple, which acted as a baseline. Figures 5.3 and 5.4 show the results of the transformation using manual annotations and automatic detection of the nipple, with a view of the MRI/MRIup data with the full body surface PCL and two closer views with only the points of the relevant breast selected on the surface PCL for visualisation purposes. For this process, PCLs were downsampled using the *pcdownsample* function from Mathworks Matlab R2016a Computer Vision System Toolbox version 7.1. It was done using the grid average algorithm with a grid of 9 mm.
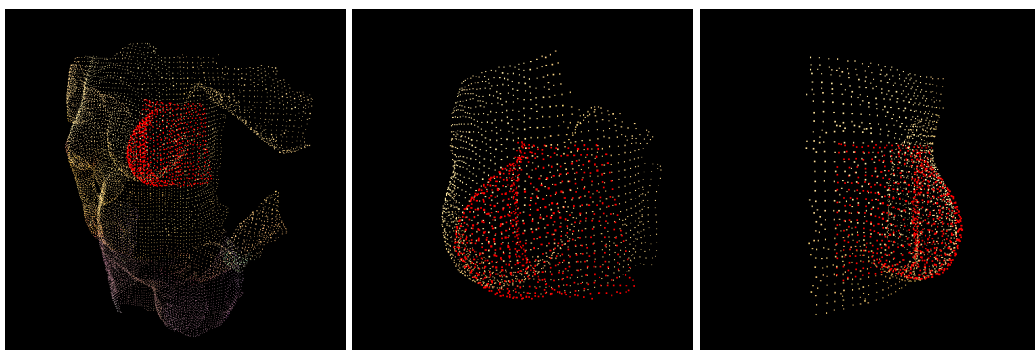
(a) MRI translation using manual annotations of the nipple.
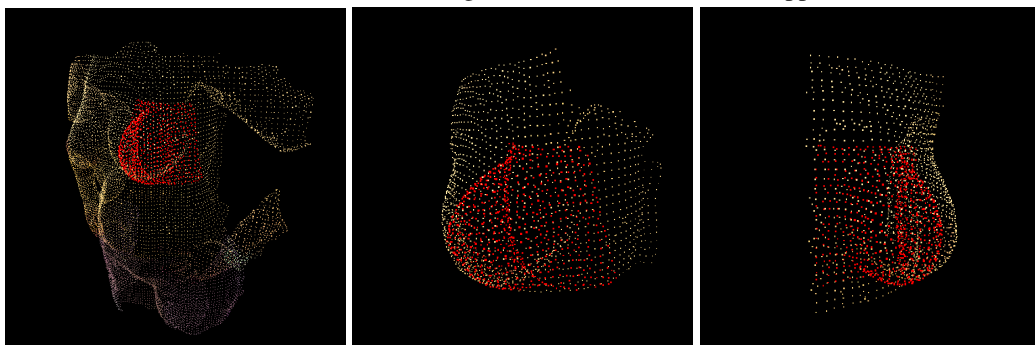
(b) MRI translation using automatic detection of the nipple.

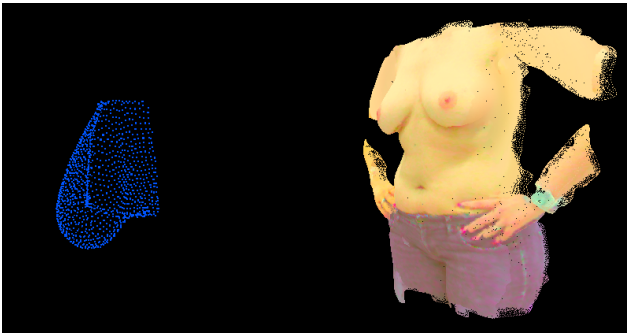Figure 5.3: Surface (natural colours) and MRI (blue) data translated using manual annotations (on the top) and automatic detection of the nipple (on the bottom). On the left is a view with the whole surface PCL, on the middle a closer view from the right side and on the left a closer view from the left side. For visualisation purposes, the surface PCL was cropped for the closer views.

It can be seen that the biomechanical simulation is more similar to the shape of the breast on the surface PCL than the MRI PCL. Analysing Figures 5.3 and 5.4, it can be observed that the translation using manual annotations gives a better approximation between PCLs than using automatic detection.

Table 5.1 displays the errors between each MRI/MRIup PCL and its corresponding surface PCL, while also displaying the mean, standard deviation (Std), maximum (Max) and minimum (Min) values. The patient identification is represented by ID and laterality differentiates the left

(a) MRIup translation using manual annotations of the nipple

(b) MRIup translation using automatic detection of the nipple.

Figure 5.4: Surface (natural colours) and MRIup (blue) data translated using manual annotations (on the top) and automatic detection of the nipple (on the bottom). On the left i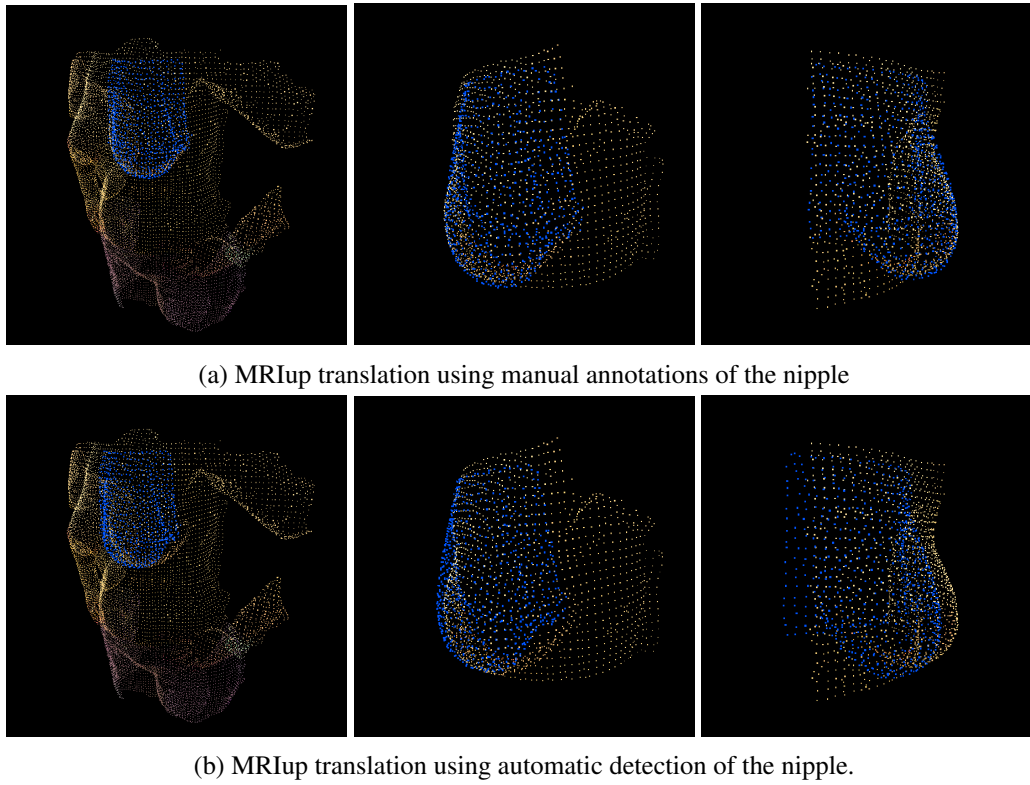s a view with the whole surface PCL, on the middle a closer view from the right side and on the left a closer view from the left side. For visualisation purposes, the surface PCL was cropped for the closer views.

Table 5.1: Distances between MRI/MRIup and surface data after translation of the MRI/MRIup PCLs using manual annotations and automatic detection of the nipple.

		Euclidean Distance (mm)				Hausdorff Distance (mm)			
		MRI		MRIup		MRI		MRIup	
ID	Laterality	Manual	Automatic	Manual	Automatic	Manual	Automatic	Manual	Automatic
1	Left	21.92	27.63	7.45	13.68	85.10	82.70	41.70	57.58
	Right	25.67	25.94	10.56	13.58	90.36	83.14	32.83	46.08
2	Right	26.52	21.96	18.86	14.81	82.53	65.88	53.70	35.32
3	Left	25.60	35.49	11.15	15.84	92.45	90.70	48.19	55.77
	Right	31.59	33.74	10.74	15.92	99.57	99.85	48.37	58.84
4	Left	19.04	20.22	9.42	9.95	66.42	66.94	32.65	32.29
5	Left	16.74	17.35	8.39	8.80	37.96	39.10	32.30	36.14
	Right	19.00	20.19	9.50	9.28	47.70	48.48	30.13	30.37
6	Left	19.56	24.90	8.90	15.65	68.75	64.18	32.95	50.32
	Right	25.06	26.33	18.67	12.32	91.87	86.49	50.83	53.67
7	Left	22.88	26.15	8.80	11.89	74.18	73.73	26.23	35.70
	Right	25.61	28.66	8.68	10.65	86.36	85.14	32.93	37.55
	Mean	23.27	25.71	10.93	12.70	76.94	73.86	38.57	44.13
	Std	4.20	5.38	3.81	2.60	18.83	17.75	9.40	10.67
	Max	31.59	35.49	18.86	15.92	99.57	99.85	53.70	58.84
	Min	16.74	17.35	7.45	8.80	37.96	39.10	26.23	30.37

and right breast. In general the distances were worse when using automatic detection. Regarding the euclidean distance, the MRI data resulted in 23.27±4.20 mm with manual annotations

of the nipple and 25.71±5.38 mm with automatic detection, while the MRIup PCL went from 10.93±3.81 mm to 12.70±2.60 mm. The Hausdorff distance when using the MRI data was the only outcome with a better average for the translation using automatic detection, going from 76.94±18.83 mm, using manual annotations, to 73.86±17.75 mm. As for the MRIup PCL, the average Hausdorff distance is 38.57±9.40 mm and 44.13±10.67 mm, using manual annotations and automatic detection respectively. This confirms that the automatic detection of the nipple is not as good as the manual annotations.

The automatic detection method is not as good as manual annotations because it does not always detect the nipple. It calculates the surface variance (SV) for each PCL and finds the minimum in the Z-axis among selected points with high SV. Figure 5.5 shows an example of this selection of points.
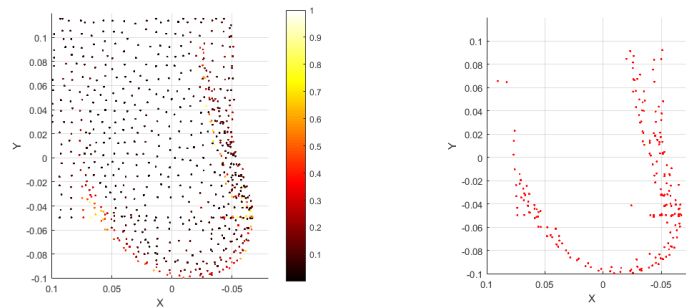
(a) SV heat map of the MRIup data (left) and the points selected (right).
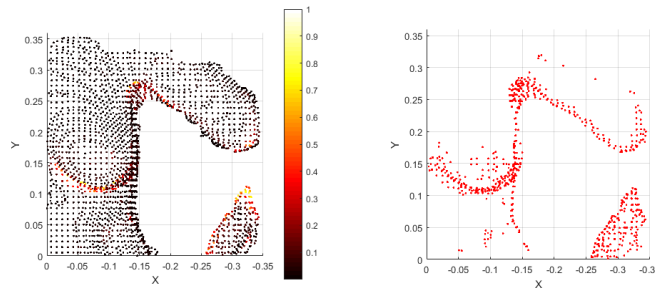
(b) SV heat map of the surface data (left) and the points selected (right).
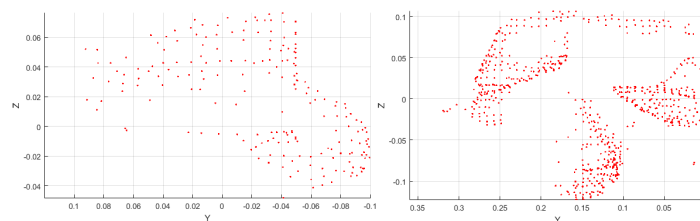
(c) Side view of the selected points of the MRIup (left) and surface (right) data.

Figure 5.5: Surface variance heat maps for MRIup (top) and surface (middle) data and comparison of the points selected (bottom).

In this case, in the MRIup PCL, only one point was selected in the area where the nipple is expected to be, while in the surface data many points were detected, so the minimum in Z might not be the nipple but in the area close to it. This means the nipple is not being detected properly, which leads to translations using automatic detection of the nipple having worse results than when using manual annotations.

To improve the approximation done by rotating and translating the MRI/MRIup data, an ICP algorithm is applied. In the next section, the results of the ICP are exposed and analysed to determine if it can better the results.

5.1.3 Rigid Iterative Closest Points

To complement the rotation and translation, a rigid ICP algorithm is applied to the MRI/MRIup data using the surface information as the reference. It compensates for the translation, especially when using automatic detection, to give an improved input for the non-rigid step of the methodology.

The ICP has different changeable parameters: the threshold for the stop condition, the maximum number of iterations, the metric for the distance minimisation and the inlier ratio.

The threshold is a two element vector $[Tdiff \ Rdiff]$, which dictates a translation and rotation tolerance. If the average from the last three iterations falls below both selected values, the algorithm stops. The tolerance used was $[0.0001 \ 0.001]$, with the translation difference being in meters and the rotation difference in radians.

The ICP algorithm will also stop if it reaches the maximum number of iterations which was set to 10000.

The metric for distance minimisation can be point to point or point to plane. Since there is not a known correspondence of points between the MRI/MRIup and surface data, the point to plane metric was chosen. This means that the distance is calculated between each point in the MRI/MRIup PCL and a plane computed using its six nearest points on the surface.

The inlier ratio is the percentage of paired points to use. For example, if a 90% inlier ratio is chosen, the bigger distances are identified as outliers in a way that only 90% of the calculated distances are used for minimisation. In the next section, the choice of inlier ratio for this implementation is discussed.

5.1.3.1 Inlier Ratio

One parameter that influences the result of the ICP algorithm is the inlier ratio, which is the percentage of paired points to use. This is useful to remove matched pairs with larger distances between them which can be incorrectly matched points.

To decide the inlier ratio value used, each MRI and MRIup, after translation using automatic detection of the nipple, went through an ICP algorithm multiple times, iteratively increasing the ratio from 60% to 100%, 5% at a time. The average euclidean distance for each inlier ratio was calculated and the ones with the lowest distance were chosen. For the MR PCL, 95% had the

smallest error, while the MRIup data had 100% as the best inlier ratio, which means all pairs are used. The results are shown in Table 5.2.

Table 5.2: Average euclidean distance between MRI/MRIup and surface after ICP with varying inlier ratios.

	Euclidean Distance (mm)	
Inlier Ratio	**MRI**	**MRIup**
0.60	16.78	11.68
0.65	16.27	10.48
0.70	15.65	10.23
0.75	14.92	9.41
0.80	14.11	8.57
0.85	13.38	8.06
0.90	13.19	7.88
0.95	**13.02**	7.83
1.00	13.10	**7.77**

5.1.3.2   ICP

Table 5.3: Distances between downsampled MRI/MRIup data (after translation using manual annotations and automatic detection of the nipple) and the surface PCLs after an ICP algorithm.

		Euclidean Distance (mm)				Hausdorff Distance (mm)			
		MRI		**MRIup**		**MRI**		**MRIup**	
ID	**Laterality**	**Manual**	**Automatic**	**Manual**	**Automatic**	**Manual**	**Automatic**	**Manual**	**Automatic**
1	Left	15.59	15.59	7.11	7.12	38.64	38.55	36.28	36.30
	Right	14.09	13.99	7.33	7.34	37.38	39.58	28.54	28.51
2	Right	11.39	11.39	8.52	8.53	31.54	31.55	23.17	23.09
3	Left	19.67	19.63	7.80	7.80	63.29	63.26	44.07	44.10
	Right	14.52	14.52	6.68	6.68	80.17	80.12	35.62	35.62
4	Left	11.34	11.29	7.20	7.20	30.86	30.66	25.72	25.73
5	Left	5.49	5.49	4.34	4.34	25.51	25.51	19.17	19.18
	Right	6.74	6.74	5.46	5.46	29.17	29.18	15.01	15.01
6	Left	13.76	10.85	7.17	7.16	42.08	49.94	29.68	29.69
	Right	19.06	17.48	7.69	8.29	55.78	54.17	31.73	27.65
7	Left	11.24	11.24	4.33	4.33	37.26	37.21	17.40	17.39
	Right	12.57	12.49	5.33	5.33	40.59	37.81	24.31	24.31
	Mean	12.95	12.56	6.58	6.63	42.69	43.13	27.56	27.21
	Std	4.22	4.05	1.38	1.44	16.01	16.05	8.53	8.44
	Max	19.67	19.63	8.52	8.53	80.17	80.12	44.07	44.10
	Min	5.49	5.49	4.33	4.33	25.51	25.51	15.01	15.01

In Table 5.3, it can be seen that the ICP algorithm gives practically the same results using the MRI/MRIup data coming from manual annotations or from automatic detection, while effectively giving a better approximation on both cases. After applying the ICP algorithm, the MRI data had an average euclidean distance of 12.95 mm, translated using manual annotations, and 12.56 mm, translated with automatic detection, while the MRIup data had 6.58 mm and 6.63 mm,

respectively. The Hausdorff distances of the translated MRI data using manual annotations were
42.69 mm and 43.13 mm for the translated MRI PCL using automatic detection. For the MRIup
data, the Hausdorff distances were 27.56 mm and 27.21 mm, respectively. These are nearly iden-
tical values, which demonstrates that the ICP algorithm can compensate for the translation using
automatic detection of the nipple not giving a great alignment, and in some cases give a better
outcome than with translated data using manual annotations. The ICP algorithm lowers consid-
erably the distances, for example, the average euclidean distances for the translated MRI/MRIup
data using automatic detection drop from 25.71/12.70 mm before the algorithm to 12.56/6.63 mm
after. As expected, it can also be observed that the MRIup data has smaller distances than the MRI
data, approximately half in the case of the euclidean distance. Visual results, Figure 5.6, further
evidentiate a better approximation when using the MRIup data as opposed to the MRI data.

(a) MRI and surface data after the ICP algorithm.

(b) MRIup and surface data after the ICP algorithm.
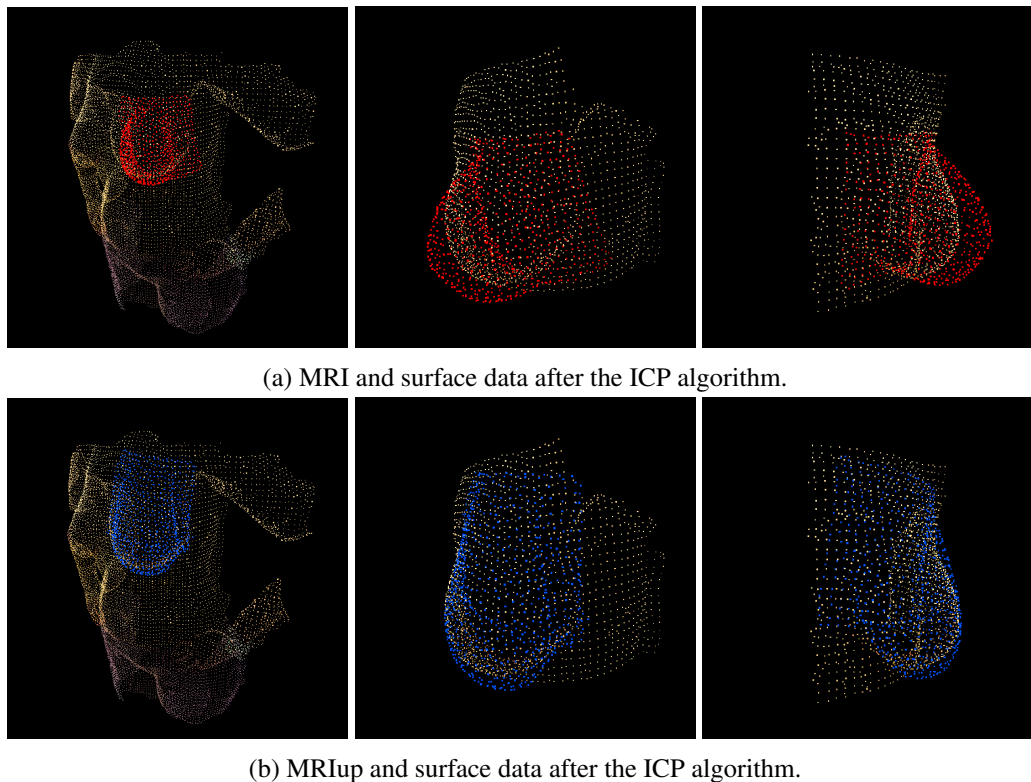
Figure 5.6: Result of applying the ICP algorithm to MRI/MRIup (red/blue) data with the surface
PCL (natural colours) as reference. On the left is a view with the whole surface PCL, on the middle
a closer view from the right side and on the left a closer view from the left side. For visualisation
purposes, the surface PCL was cropped for the closer views.

5.2   Non-Rigid Registration

A good alignment from the previous step is important because the non-rigid registration, which
consists of an FFD algorithm, iteratively minimises the distance of the closest points between the

MRI/MRIup and surface information. A good rigid transformation helps to ensure that the closest points in the MRI/MRIup and surface PCL are of the same area of the breast.

5.2.1 Free Form Deformation

For the FFD, the parameters that can be changed are the size of the control point grid, the threshold to stop the algorithm (euclidean distance between the current MRI/MRIup PCL and from the previous iteration) and the maximum number of iterations. Regarding the grid, different sizes were experimented for comparison. The threshold chosen is zero, which means the FFD stops when there is no change on the MRI/MRIup PCL between iterations. The maximum number of iterations is 300, which is, in most cases, more than the number needed to reach the threshold.

First, the FFD was applied on downsampled PCLs and the surface PCL was cropped around the MRIup data for a faster computation time. Different sizes of control point grids, both 2D and 3D, were experimented and compared, namely [6 6 0], [6 6 6], [8 8 0] and [8 8 8]. For this study only the MRIup PCLs were utilised, since they presented better results after the ICP algorithm. The distances and the time to compute each PCL are presented on Table 5.4 and 5.5, respectively.

Table 5.4: Distances between downsampled MRIup and surface data after FFD.

ID	Laterality	Euclidean Distance (mm)				Hausdorff Distance (mm)			
		[6 6 0]	[6 6 6]	[8 8 0]	[8 8 8]	[6 6 0]	[6 6 6]	[8 8 0]	[8 8 8]
1	Left	1.19	1.44	1.04	1.04	6.97	11.10	6.07	7.08
	Right	1.21	1.46	0.95	1.02	6.04	9.28	5.97	6.38
2	Right	1.60	1.31	1.33	0.96	5.15	7.44	5.07	5.68
3	Left	1.36	1.85	1.20	1.47	4.87	19.87	6.06	14.23
	Right	1.57	1.77	1.29	1.34	5.59	10.91	5.74	9.74
4	Left	1.07	1.42	1.10	1.10	4.31	8.23	4.51	6.44
5	Left	1.31	1.42	1.41	1.07	8.44	7.48	7.04	5.41
	Right	1.54	1.39	1.23	1.03	7.87	5.55	7.22	4.70
6	Left	1.26	1.23	1.11	0.95	6.48	7.00	5.32	4.80
	Right	1.38	1.19	1.12	0.92	5.41	6.46	5.18	4.45
7	Left	1.07	1.38	1.09	1.03	5.35	7.41	5.52	6.37
	Right	1.28	1.46	1.24	1.09	6.88	7.95	5.37	5.99
	Mean	1.32	1.44	1.18	**1.08**	6.11	9.06	**5.76**	6.77
	Std	0.18	0.19	0.13	0.16	1.25	3.78	0.78	2.73
	Max	1.60	1.85	1.41	1.47	8.44	19.87	7.22	14.23
	Min	1.07	1.19	0.95	0.92	4.31	5.55	4.51	4.45

Table 5.4 shows that the [8 8 8] control point grid had the best results, but both 2D grids were better than the [6 6 6] grid. However the visual outcome from both 2D grids is not very accurate. When analysing figure 5.7, it can be observed that the MRIup PCL does not completely cover the breast when registered using a 2D control point grid. Even though the [6 6 6] grid presented the worst results (1.44 mm compared to 1.32 mm with [6 6 0] grid and 1.18 mm with a [8 8 0] grid), it visually looks like a better registration than both 2D grids. The [8 8 8] grid resulted in the

Table 5.5: Computation time of the FFD applied to downsampled MRIup and surface PCLs.

| ID	Laterality	Time (seconds) [6 6 0]	[6 6 6]	[8 8 0]	[8 8 8]
1	Left	89.02	160.10	57.34	280.74
	Right	38.79	256.01	42.06	192.70
2	Right	40.21	83.42	77.69	131.70
3	Left	64.27	245.45	107.56	557.68
	Right	72.47	110.09	118.05	534.77
4	Left	61.83	149.32	89.51	214.91
5	Left	50.23	112.52	82.64	137.25
	Right	27.79	75.01	42.72	183.23
6	Left	50.90	85.76	78.28	287.01
	Right	48.89	96.26	112.08	203.31
7	Left	75.56	85.84	131.03	270.93
	Right	74.34	162.18	118.36	253.10
	Mean	57.86	135.16	88.11	270.61
	Std	18.07	61.90	30.11	138.59
	Max	89.02	256.01	131.03	557.68
	Min	27.79	75.01	42.06	131.70

best average euclidean distance, 1.08 mm, since, with more control points, fewer MRIup points are being controlled by each control point, giving better precision when minimising the distances between the MRIup and surface PCLs. The Hausdorff distance is a problem for the 3D grids since both 2D grids resulted in smaller Hausdorff distances, although the difference is small when using the [8 8 8] grid. This difference can be attributed to both of patient 3's breast PCLs which result in a considerable Hausdorff distance when compared to the rest of the sample. Excluding the patient 3 from the sample, the mean Hausdorff distance for the [8 8 8] grid falls from 6.77 mm to 5.73 mm and the standard deviation from 2.73 mm to 0.88 mm. Another disadvantage of 3D control point grids is the time it takes to complete the FFD algorithm, as established in Table 5.5.
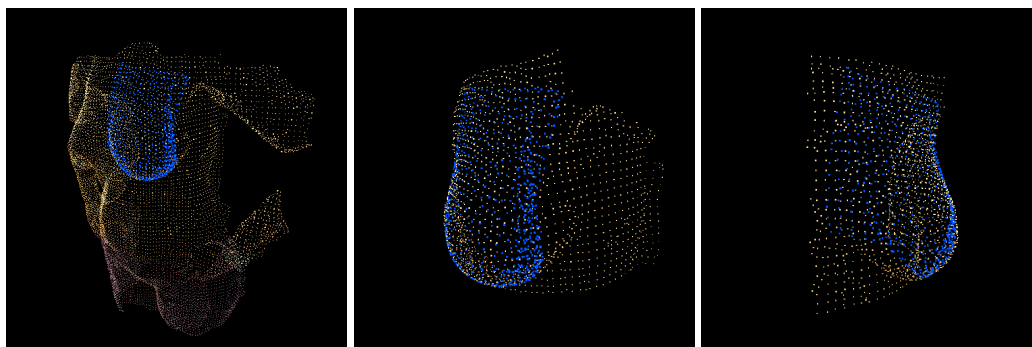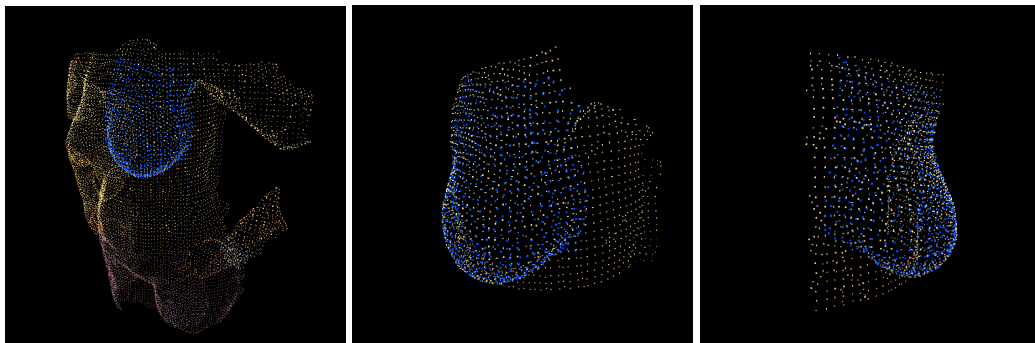

(a) MRIup and surface data after FFD algorithm with a [6 6 0] control point grid.
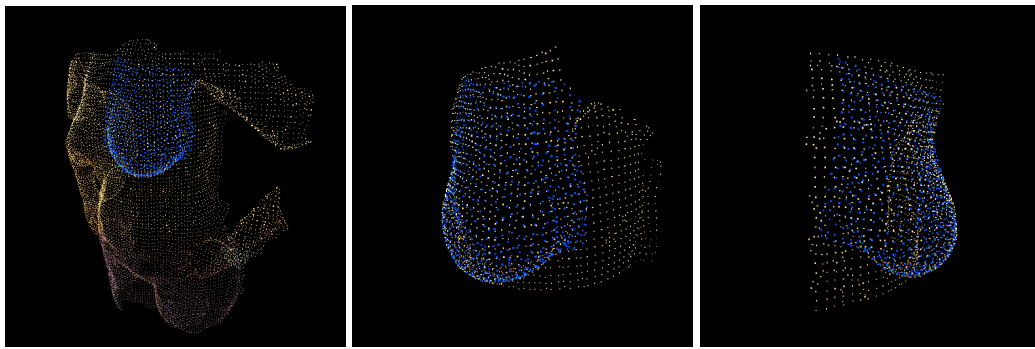
(b) MRIup and surface data after FFD algorithm with a [6 6 6] control point grid.
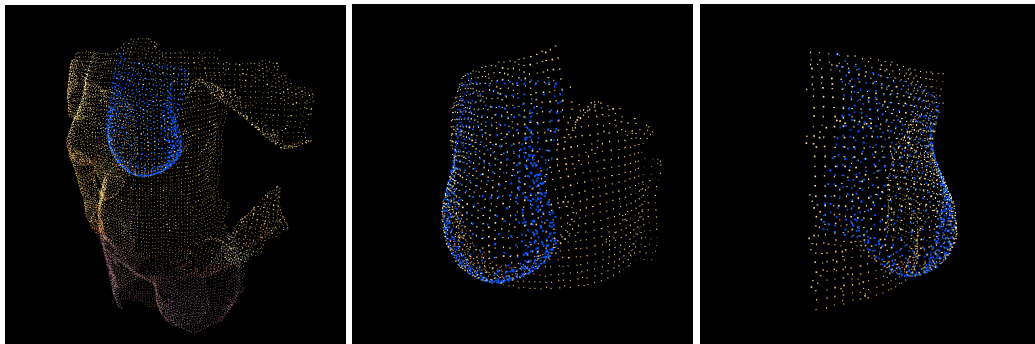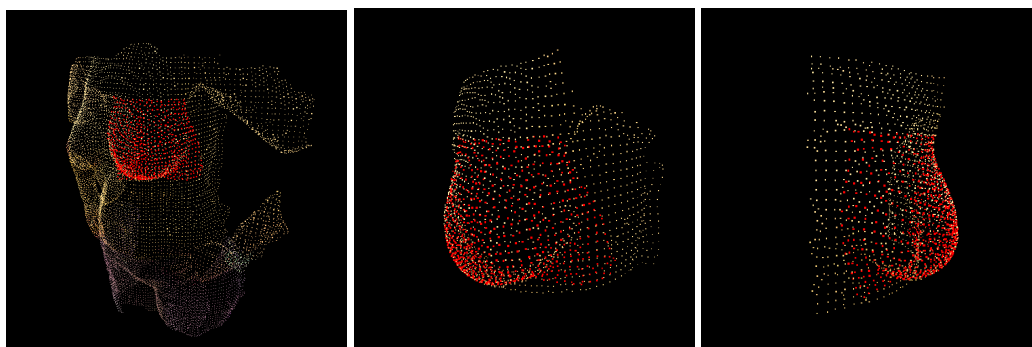

(c) MRIup and surface data after FFD algorithm with a [8 8 0] control point grid.

(d) MRIup and surface data after the FFD algorithm with a [8 8 8] control point grid.

Figure 5.7: Result of applying the FFD algorithm to a downsampled MRIup PCL with [6 6 0] (top), [6 6 6] (upper middle), [8 8 0] (lower middle) and [8 8 8] (bottom) control point grid. On the left is a view with the whole surface PCL, on the middle a closer view from the right side and on the left a closer view from the left side.

To determine if the biomechanical simulations are necessary to achieve good results, the FFD algorithm with a [8 8 8] control point grid was applied on the MRI data. Figure 5.8 displays the resulting PCL. Considering the shape of the MRI data is different than the MRIup, the result of the FFD algorithm is also different, but still a good approximation of the surface PCL. The results (distances and times) are exposed in Table 5.6. It can be observed that the errors are bigger compared to using the MRIup data, which is to be expected since the starting shape is not as similar to the surface. The average euclidean distance is 1.46 mm, while, in the same conditions, the MRIup data resulted in 1.08 mm. Therefore it can be concluded that the biomechanical simulations, lead

(a) MRI and surface data after the FFD algorithm with a [8 8 8] control point grid.

Figure 5.8: Result of applying the FFD algorithm to a downsampled MRI PCL with a [8 8 8] control point grid. On the left is a view with the whole surface PCL, on the middle a closer view from the right side and on the left a closer view from the left side.

to better results, however further analysis is necessary to determine if the resulting shape is physically more correct with MRI or MRIup data, such as volume comparison before and after the FFD algorithm.

Table 5.6: Results (distances and times) from applying the FFD algorithm to downsampled MRI and surface data.

| ID | Laterality | Distances (mm) | | Time |
		Euclidean	Hausdorff	(seconds)
1	Left	1.40	8.86	551.77
	Right	1.51	8.56	654.98
2	Right	1.15	6.26	200.43
3	Left	2.00	12.12	818.34
	Right	1.72	12.29	712.38
4	Left	1.50	10.15	246.01
5	Left	1.15	6.98	178.22
	Right	1.14	5.33	122.41
6	Left	1.17	5.13	192.30
	Right	1.66	9.65	872.29
7	Left	1.52	8.51	266.31
	Right	1.55	9.29	252.05
	Mean	1.46	8.59	422.29
	Std	0.27	2.35	278.05
	Max	2.00	12.29	872.29
	Min	1.14	5.13	122.41

In order to try and decrease the error further, the FFD was applied to the MRIup and surface PCLs without downsampling, using a [6 6 6] and a [8 8 8] control point grid. Since the algorithm matches the closest points between PCLs, with more points, it is probable that there will be better correspondence between points of the MRIup and surface PCL.

Figure 5.9 shows the resulting PCLs. The distance results are exposed on Table 5.7, which

demonstrates that the mean euclidean distance with both grids is lower than with downsampled PCLs, 1.05 mm for the [6 6 6] grid and 0.83 mm for the [8 8 8] grid. The latter has the best result for both metrics, with a average Hausdorff distance of 5.06 mm. The standard deviation for the Hausdorff distance is 2.50 mm and is mainly due to the patient 3's left breast PCL, which has a 12.53 mm Hausdorff distance. It is also giving the worst euclidean distance at 1.02 mm. Without this exception, the average Hausdorff distance would be 4.38±0.89 mm.

With the mean euclidean distance at 0.83±0.10 mm and the average Hausdorff ditance at 5.06±2.50 mm, the FFD algorithm applied on the MRIup and surface data without downsampling gives the best results. However the average duration to compute the registered PCL is much higher, going from 270,61 to 3016,72 seconds, as can be seen in Table 5.8. Due to having more points to match, each iteration takes more time to complete, and the FFD algorithm needs more iterations to reach the threshold because there is less change between iterations. This is also the reason the FFD using the grid with less points has a longer duration on average, because it has more difficulty in reaching the threshold, needing more iterations.
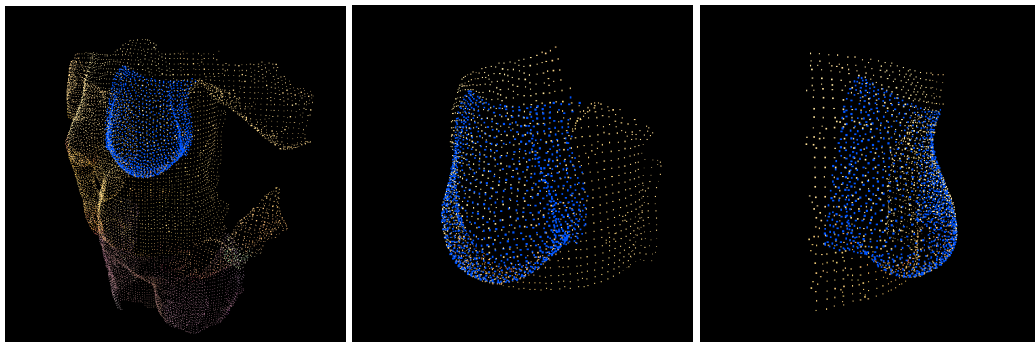
(a) MRIup and surface data after the FFD algorithm with a [6 6 6] control point grid.
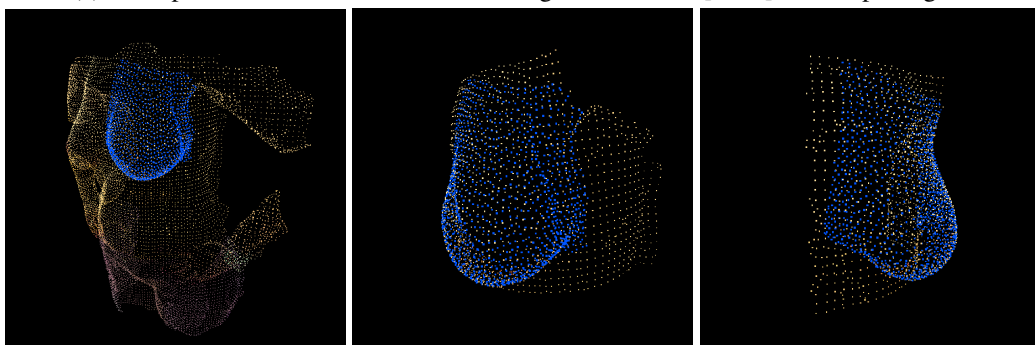
(b) MRIup and surface data after the FFD algorithm with a [8 8 8] control point grid.

Figure 5.9: Result of applying the FFD algorithm to a MRIup PCL without downsampling with a [6 6 6] and [8 8 8] control point grid.

Table 5.7: Distances between MRIup and surface data after FFD.

ID	Laterality	Euclidean Distance (mm)		Hausdorff Distance (mm)	
		[6 6 6]	**[8 8 8]**	**[6 6 6]**	**[8 8 8]**
1	Left	1.10	0.88	7.46	5.63
	Right	1.12	0.88	7.91	5.33
2	Right	0.80	0.67	3.71	3.09
3	Left	1.38	1.02	16.49	12.53
	Right	1.09	0.91	7.51	3.78
4	Left	0.96	0.73	4.64	3.39
5	Left	1.09	0.84	5.32	4.57
	Right	0.83	0.78	3.04	3.24
6	Left	0.99	0.78	6.30	4.25
	Right	0.94	0.74	6.58	4.98
7	Left	1.18	0.92	5.71	4.93
	Right	1.09	0.87	6.60	5.00
	Mean	1.05	**0.83**	6.77	**5.06**
	Std	0.16	0.10	3.41	2.50
	Max	1.38	1.02	16.49	12.53
	Min	0.80	0.67	3.04	3.09

Table 5.8: Computation time of the FFD applied to MRIup and surface PCLs.

ID	Laterality	Time (seconds)	
		[6 6 6]	**[8 8 8]**
1	Left	4127.92	4448.37
	Right	3266.04	2259.99
2	Right	3991.62	2427.78
3	Left	5832.80	6071.50
	Right	5564.83	2321.21
4	Left	4198.64	2952.95
5	Left	2735.67	2119.15
	Right	5231.18	4149.05
6	Left	2939.08	3270.43
	Right	2459.28	1384.71
7	Left	2489.20	2338.94
	Right	4368.07	2456.59
	Mean	3933.69	3016.72
	Std	1182.50	1292.54
	Max	5832.80	6071.50
	Min	2459.28	1384.71

5.3 Discussion

The rigid registration step involving a rotation, translation and ICP algorithm is successful in supplying a good alignment between the MRI/MRIup PCL. Nonetheless, this step can be improved.

The rotation should not depend on the input data always having the same orientation. An improvement to this step would be orientation detection to ensure the right alignment even if the input data does not have the expected orientation.

The translation is done with automatic detection of the nipple but, when compared with translation using manual annotations, it gives worse results. A better way to detect the breast could be an improvement, however, it can be argued that it would be unnecessary, since the ICP algorithm compensates for the automatic translation.

Regarding the non-rigid registration step, various control point grids were tested. With only downsampled MRIup PCLs, the use of 2D and 3D control point grids was compared, particularly [6 6 0], [6 6 6], [8 8 0] and [8 8 8]. Due to memory limitations of Matlab, grids with more control points could not be tested. The 2D grids, although having good results in both distances and time, do not give an accurate outcome. Although the MRIup points end up close to the surface PCL, they are not well spread over the breast, not having points on the edges. The main advantage of the 2D grids is the computation time, which is considerably smaller because of the fewer control points. With 3D control point grids, the results are visually better. As for distances, the [8 8 8] control point grid has better results regarding the euclidean distance (1.08 ± 0.16 mm), but is still behind the 2D grids when it comes to the Hausdorff distance (6.77 ± 2.73 compared to 5.76 ± 0.78 using a [8 8 0] grid), mainly because the PCLs of the patient 3 have much worse results than the rest of the sample (14.23 and 9.74 mm for the left and right breast respectively). Patient 3's left breast PCL also results in the maximum euclidean distance when using the 3D control point grids. The reason this happens is that the rigid registration does not result in a good enough approximation in this case, therefore the FFD does not work as intended.

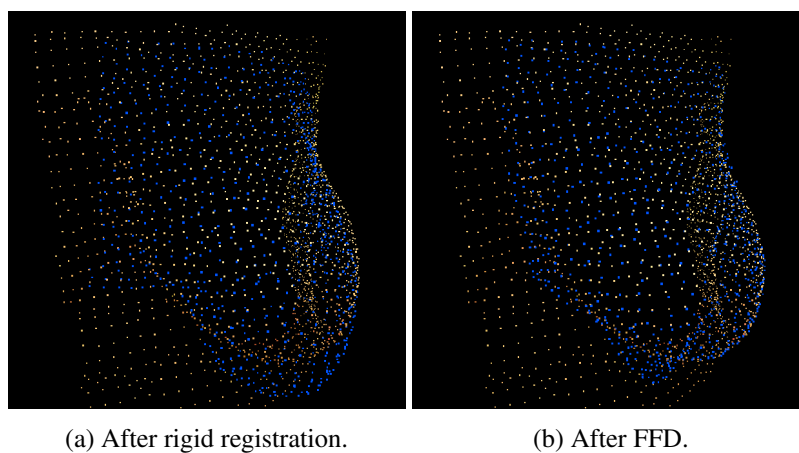(a) After rigid registration.   (b) After FFD.

Figure 5.10: Result of applying the FFD algorithm to the downsampled MRIup PCL of the patient 3's left breast with a [8 8 8] control point grid.

Figure 5.10 shows the result of the FFD algorithm on the downsampled MRIup of the patient 3's left breast and its respective surface PCLs with a [8 8 8] grid. It can be observed that before applying the FFD algorithm, the PCLs are not aligned well enough, which means the rigid registration step did not give a good enough result in this case. The points on the bottom of the MRIup PCL are matched with the points on the skin below the breast, since they are the closest. One way to solve this problem would be to calculate the displacement field between each point on the MRI/MRIup and the point in the direction of its inward facing normal, as suggested by [3] and illustrated in Figure 5.11. What the algorithm does is match M to P' (closest points), but, using inward normals, it could match to P. This way the bottom of the MRIup PCL would be mapped to the bottom part of the breast on the surface instead of the skin below.
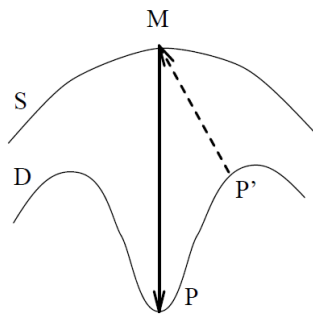

Figure 5.11: Comparison between matching closest points or points in the inward normal direction (from [3]).

The FFD algorithm was also applied to downsampled MRI PCLs, albeit only with a [8 8 8] control point grid. When compared with the MRIup PCLs, the results are worse in all categories with a 1.46±0.27 mm average euclidean distance, compared to 1.08±0.16 mm from the MRIup, and a 8.59±2.35 mm average Hausdorff distance, compared to 6.77±2.73 mm from the MRIup. This is expected because the MRI PCL is not as similar to the surface, so the rigid registration does not work as well. Because of this, the points on the MRI and surface data are farther apart, which can lead to points being incorrectly matched. The MRIup data can achieve a better rigid approximation, since the biomechanical model compensates for the pose difference, and enters the FFD algorithm closer to the surface, leading to better results.

Using the MRIup and surface PCLs without downsampling was also tested. With this, the best results were achieved, when applying the FFD algorithm with a [8 8 8] control point grid. The mean euclidean distance was 0.83±0.10 mm and the average Hausdorff distance was 5.06±2.50 mm. However the computation time of the algorithm is much longer compared to the downsampled PCLs, with the average time going from 270,61 to 3016,72 seconds. Having more points to match, the FFD algorithm results in a closer match to the reference, but each iteration is slower and more iterations are needed to reach the threshold.

The work of Salmon et al. [38], is also on matching breast MRI and surface data, although using a purely biomechanical approach. They achieved an error of 2 mm, testing on only one patient, while with this dissertation, lower errors were achieved with a sample of twelve breasts.

The results from this methodology are promising, achieving a 0.83±0.10 mm mean euclidean distance with a sample of 12 breast PCLs. However, the computation time to achieve these results is considerable. The computation time can be lowered with the trade-off of the distances getting bigger. Therefore, different parameters can be chosen depending on the application, which might need faster or more precise results.

Chapter 6

Conclusions

Breast cancer is a terrible disease that affects millions of women worldwide. Although the survival rates are high, especially when found early, the treatment, almost always including surgery, leads to deformations in the breast. This results in many patients developing body image problems, which has a negative psychosocial effect. Studies show that when both the patients and doctors are involved in the treatment decision process, there are less negative effects, which highlights the importance of having good surgical planning tools.

Image registration can be a powerful tool in a clinical setting for visualising imaging data, by combining complementary information from various sources. Breast image registration between radiological modalities is a popular research topic, but few work has been done with exterior and interior registration. With this dissertation, a methodology that matches MRI and surface information was implemented in a two part process to counteract the breast shape differences inherent to the distinct poses of the patient when the data is acquired. First a rigid registration is applied to align the MRI/MRIup PCLs with the surface data. It involves a rotation, translation and a rigid ICP algorithm. Due to the deformable nature of the breast, a non-rigid registration is also necessary to compensate for the difference in the shapes of the MRI/MRIup and surface information. An FFD algorithm was applied after the rigid transformations and the results are promising.

6.1 Future Work

The results of this dissertation are promising in a topic with few research done, but there are still improvements to the methodology that can be implemented.

The rotation should be done with orientation detection, so that it does not depend on the data being in a certain way.

The automatic detection of the nipple could be improved, since it does not always result in a good translation.

The ICP algorithm has a few changeable parameters and a study to determine which parameters give better results should be done, similar to what was done for the inlier ratio.

The data of one patient consistently has the worst results, which happens because the rigid registration does not give a good enough approximation for the FFD algorithm to work as intended. The improvements to the rigid registration already mentioned could solve this problem or the FFD algorithm could be altered to be successful even in this case and others similar to this one.

There is also future work to be done beyond improvements of the steps already discussed. Further validation is needed to determine how robust the methodology is. An approach to validate could be using synthetic validation, which means applying known deformations and/or noise to a PCL and utilising the methodology on the transformed and original PCLs, using the deformed data as the reference and ground truth.

Volume calculation and comparison before and after the FFD algorithm could be done to verify if the deformations applied on the MRI/MRIup data are physically correct.

An important step that is missing is the deformation of the interior points of the MRI/MRIup PCLs, to match the deformation of the exterior points, in order to have the registered breast complete with exterior and interior information.

This registration is important for the creation of a complete 3D model of the breast, that can have a clinical application as a patient specific tool for visualisation.

References

[1] L Aerts, MR Christiaens, Paul Enzlin, Patrick Neven, and Frédéric Amant. Sexual functioning in women after mastectomy versus breast conserving therapy for early-stage breast cancer: a prospective controlled study. *The breast*, 23(5):629–636, 2014.

[2] Gheonea Ioana Andreea, Raluca Pegza, Luana Lascu, Simona Bondari, Zoia Stoica, and A Bondari. The role of imaging techniques in diagnosis of breast cancer. *J. Curr. Health Sci*, 37(2):241–248, 2011.

[3] Eric Bardinet, Laurent D Cohen, and Nicholas Ayache. A parametric deformable model to fit unstructured 3d data. *Computer vision and image understanding*, 71(1):39–54, 1998.

[4] Christian Behrenbruch, Kostas Marias, Paul Armitage, Niall Moore, Jane Clarke, and JM Brady. Prone-supine breast mri registration for surgical visualisation. In *Medical Image Understanding and Analysis*, 2001.

[5] David T Chen, Ioannis A Kakadiaris, Michael J Miller, R Bowen Loftin, and Charles Patrick. Modeling for plastic and reconstructive breast surgery. In *MICCAI*, pages 1040–1050. Springer, 2000.

[6] Pedro Costa, João P Monteiro, Hooshiar Zolfagharnasab, and Hélder P Oliveira. Tessellation-based coarse registration method for 3d reconstruction of the female torso. In *Bioinformatics and Biomedicine (BIBM), 2014 IEEE International Conference on*, pages 301–306. IEEE, 2014.

[7] Pedro Miguel Ferro da Costa. Kinect based system for breast 3d reconstruction. 2014.

[8] Carol E DeSantis, Jiemin Ma, Ann Goding Sauer, Lisa A Newman, and Ahmedin Jemal. Breast cancer statistics, 2017, racial disparity in mortality by state. *CA: a cancer journal for clinicians*, 67(6):439–448, 2017.

[9] Jennifer S Drukteinis, Blaise P Mooney, Chris I Flowers, and Robert A Gatenby. Beyond mammography: new frontiers in breast cancer screening. *The American journal of medicine*, 126(6):472–479, 2013.

[10] Björn Eiben, Vasileios Vavourakis, John H Hipwell, Sven Kabus, Cristian Lorenz, Thomas Buelow, Norman R Williams, M Keshtgar, and David J Hawkes. Surface driven biomechanical breast image registration. In *Medical Imaging 2016: Image-Guided Procedures, Robotic Interventions, and Modeling*, volume 9786, page 97860W. International Society for Optics and Photonics, 2016.

[11] J Ferlay, I Soerjomataram, Morten Ervik, Rajesh Dikshit, Sultan Eser, C Mathers, M Rebelo, DM Parkin, David Forman, and Freddie Bray. GLOBOCAN 2012 v1.0, Cancer Incidence

and Mortality Worldwide: IARC Cancer Base No. 11 [Internet]. Lyon, France: International Agency for Research on Cancer; 2013 Available from: http://globocan.iarc.fr.

[12] Martin Fuhry and Lothar Reichel. A new tikhonov regularization method. *Numerical Algorithms*, 59(3):433–445, 2012.

[13] Yujun Guo, Jasjit Suri, and Radhika Sivaramakrishna. Image registration for breast imaging: a review. In *Engineering in Medicine and Biology Society, 2005. IEEE-EMBS 2005. 27th Annual International Conference of the*, pages 3379–3382. IEEE, 2006.

[14] Lianghao Han, John H Hipwell, Bjorn Eiben, Dean Barratt, Marc Modat, Sebastien Ourselin, and David J Hawkes. A nonlinear biomechanical model based registration method for aligning prone and supine mr breast images. *IEEE transactions on medical imaging*, 33(3):682–694, 2014.

[15] John H Hipwell, Christine Tanner, William R Crum, Julia A Schnabel, and David J Hawkes. A new validation method for x-ray mammogram registration algorithms using a projection model of breast x-ray compression. *IEEE Transactions on Medical Imaging*, 26(9):1190–1200, 2007.

[16] John H Hipwell, Vasileios Vavourakis, Lianghao Han, Thomy Mertzanidou, Björn Eiben, and David J Hawkes. A review of biomechanically informed breast image registration. *Physics in medicine and biology*, 61(2):R1, 2016.

[17] Ilyang Joo, Kanghun Jeong, et al. Breast image registration for pet-ct and mr based on 3d surface matching. *International Journal of Bio-Science and Bio-Technology*, 5(6):201–206, 2013.

[18] Yasuyo Kita, Ralph Highnam, and Michael Brady. Correspondence between different view breast x-rays using a simulation of breast deformation. In *Computer Vision and Pattern Recognition, 1998. Proceedings. 1998 IEEE Computer Society Conference on*, pages 700–707. IEEE, 1998.

[19] Yasuyo Kita, Ralph Highnam, and Michael Brady. Correspondence between different view breast x rays using curved epipolar lines. *Computer vision and image understanding*, 83(1):38–56, 2001.

[20] Julia Krüger, Jan Ehrhardt, Arpad Bischof, and Heinz Handels. Breast compression simulation using icp-based b-spline deformation for correspondence analysis in mammography and mri datasets. In *Medical Imaging: Image Processing*, page 86691D, 2013.

[21] M Kuhlmann, EC Fear, A Ramirez-Serrano, and S Federico. Mechanical model of the breast for the prediction of deformation during imaging. *Medical engineering & physics*, 35(4):470–478, 2013.

[22] Angela Lee, Julia Schnabel, Vijay Rajagopal, Poul Nielsen, and Martyn Nash. Breast image registration by combining finite elements and free-form deformations. *Digital Mammography*, pages 736–743, 2010.

[23] Robert Martí, Caroline ME Rubin, Erika Denton, and Reyer Zwiggelaar. Mammographic x-ray and mr correspondence. In *Digital Mammography*, pages 527–529. Springer, 2003.

[24] Thomy Mertzanidou, John Hipwell, Stian Johnsen, Lianghao Han, Bjoern Eiben, Zeike Taylor, Sebastien Ourselin, Henkjan Huisman, Ritse Mann, Ulrich Bick, et al. Mri to x-ray mammography intensity-based registration with simultaneous optimisation of pose and biomechanical transformation parameters. *Medical image analysis*, 18(4):674–683, 2014.

[25] Elizabeth Miller, Hee Jin Lee, Amriti Lulla, Liz Hernandez, Prashanth Gokare, and Bora Lim. Current treatment of early breast cancer: adjuvant and neoadjuvant therapy. *F1000Research*, 3, 2014.

[26] Theo Moons, Luc Van Gool, Maarten Vergauwen, et al. 3d reconstruction from multiple images part 1: principles. *Foundations and Trends® in Computer Graphics and Vision*, 4(4):287–404, 2010.

[27] Rachel L O'Connell, Roger JG Stevens, Paul A Harris, and Jennifer E Rusby. Review of three-dimensional (3d) surface imaging for oncoplastic, reconstructive and aesthetic breast surgery. *The Breast*, 24(4):331–342, 2015.

[28] Francisco PM Oliveira and Joao Manuel RS Tavares. Medical image registration: a review. *Computer methods in biomechanics and biomedical engineering*, 17(2):73–93, 2014.

[29] Diogo Pernes, Jaime S Cardoso, and Hélder P Oliveira. Fitting of superquadrics for breast modelling by geometric distance minimization. In *Bioinformatics and Biomedicine (BIBM), 2014 IEEE International Conference on*, pages 293–296. IEEE, 2014.

[30] Vijay Rajagopal, Angela Lee, Jae-Hoon Chung, Ruth Warren, Ralph P Highnam, Martyn P Nash, and Poul MF Nielsen. Creating individual-specific biomechanical models of the breast for medical image analysis. *Academic Radiology*, 15(11):1425–1436, 2008.

[31] Gregory P Reece, Fatima Merchant, Johnny Andon, Hamed Khatam, K Ravi-Chandar, June Weston, Michelle C Fingeret, Chris Lane, Kelly Duncan, and Mia K Markey. 3d surface imaging of the human female torso in upright to supine positions. *Medical engineering & physics*, 37(4):375–383, 2015.

[32] Fabio Remondino and Sabry El-Hakim. Image-based 3d modelling: A review. *The Photogrammetric Record*, 21(115):269–291, 2006.

[33] Daniel Rueckert, Carmel Hayes, Colin Studholme, Paul Summers, M Leach, and David J Hawkes. Non-rigid registration of breast mr images using mutual information. In *International Conference on Medical Image Computing and Computer-Assisted Intervention*, pages 1144–1152. Springer, 1998.

[34] Daniel Rueckert and Julia A Schnabel. Registration and segmentation in medical imaging. In *Registration and Recognition in Images and Videos*, pages 137–156. Springer, 2014.

[35] Daniel Rueckert, Luke I Sonoda, Carmel Hayes, Derek LG Hill, Martin O Leach, and David J Hawkes. Nonrigid registration using free-form deformations: application to breast mr images. *IEEE transactions on medical imaging*, 18(8):712–721, 1999.

[36] Nicole V Ruiter, Rainer Stotzka, T-O Muller, Hartmut Gemmeke, Jürgen R Reichenbach, and Werner A Kaiser. Model-based registration of x-ray mammograms and mr images of the female breast. *IEEE Transactions on Nuclear Science*, 53(1):204–211, 2006.

[37] Radu Bogdan Rusu. Semantic 3d object maps for everyday manipulation in human living environments. *KI-Künstliche Intelligenz*, 24(4):345–348, 2010.

[38] Remi Salmon, Thanh Chau Nguyen, Linda W Moore, Barbara L Bass, and Marc Garbey. Multimodal imaging of the breast to retrieve the reference state in the absence of gravity using finite element modeling. In *International Conference on Innovation in Medicine and Healthcare*, pages 254–263. Springer, 2017.

[39] Giovanna Sansoni, Marco Trebeschi, and Franco Docchio. State-of-the-art and applications of 3d imaging sensors in industry, cultural heritage, medicine, and criminal investigation. *Sensors*, 9(1):568–601, 2009.

[40] Julia A Schnabel, Christine Tanner, AD Castellano Smith, Andreas Degenhard, Carmel Hayes, Martin O Leach, D Rodney Hose, Derek LG Hill, and David J Hawkes. Validation of non-rigid registration of contrast-enhanced mr mammography using finite element methods. In *Bildverarbeitung für die Medizin 2002*, pages 143–146. Springer, 2002.

[41] Radhika Sivaramakrishna. 3d breast image registration—a review. *Technology in cancer research & treatment*, 4(1):39–48, 2005.

[42] Aristeidis Sotiras, Christos Davatzikos, and Nikos Paragios. Deformable medical image registration: A survey. *IEEE transactions on medical imaging*, 32(7):1153–1190, 2013.

[43] Gary KL Tam, Zhi-Quan Cheng, Yu-Kun Lai, Frank C Langbein, Yonghuai Liu, David Marshall, Ralph R Martin, Xian-Fang Sun, and Paul L Rosin. Registration of 3d point clouds and meshes: a survey from rigid to nonrigid. *IEEE transactions on visualization and computer graphics*, 19(7):1199–1217, 2013.

[44] Lisa Tang, Ghassan Hamarneh, and K Iniewski. Medical image registration: a review. *Medical Imaging: Technology and Applications*, 1:619–660, 2013.

[45] Xu Tingting and Wei Ning. Non-rigid multi-modal medical image registration: A review. In *3rd International Conference on Multimedia Technology (ICMT-13)*. Atlantis Press, 2013.

[46] Tímea Tőkés, László Torgyík, Gyöngyvér Szentmártoni, Krisztián Somlai, Andrea Tóth, Janina Kulka, and Magdolna Dank. Primary systemic therapy for breast cancer: Does the patient's involvement in decision-making create a new future? *Patient education and counseling*, 98(6):695–703, 2015.

[47] Hooshiar Zolfagharnasab, Sílvia Bessa, Sara P Oliveira, Pedro Faria, João F Teixeira, Jaime S Cardoso, and Hélder P Oliveira. A regression model for predicting shape deformation after breast conserving surgery. *Sensors*, 18(1):167, 2018.

[48] Hooshiar Zolfagharnasab, Jaime S Cardoso, and Hélder P Oliveira. Fitting of breast data using free form deformation technique. In *International Conference Image Analysis and Recognition*, pages 608–615. Springer, 2016.